Journal of Medicinal Chemistry

pubs.acs.org/jmc

Article

Switching a Xanthine Oxidase Inhibitor to a Dual-Target Antagonist of $P2Y_1$ and $P2Y_{12}$ as an Oral Antiplatelet Agent with a Wider Therapeutic Window in Rats than Ticagrelor

Yu Lei,[‖] Bing Zhang,[‖] Dan Liu, Jian Zhao, Xiwen Dai, Jun Gao, Qing Mao, Yao Feng, Jiaxing Zhao, Fengwei Lin, Yulin Duan, Yan Zhang, Ziyang Bao, Yuwei Yang, Yanhua Mou,* and Shaojie Wang*

Cite This: https://dx.doi.org/10.1021/acs.jmedchem.0c01524

Read Online

ACCESS | Metrics & More | Article Recommendations | Supporting Information

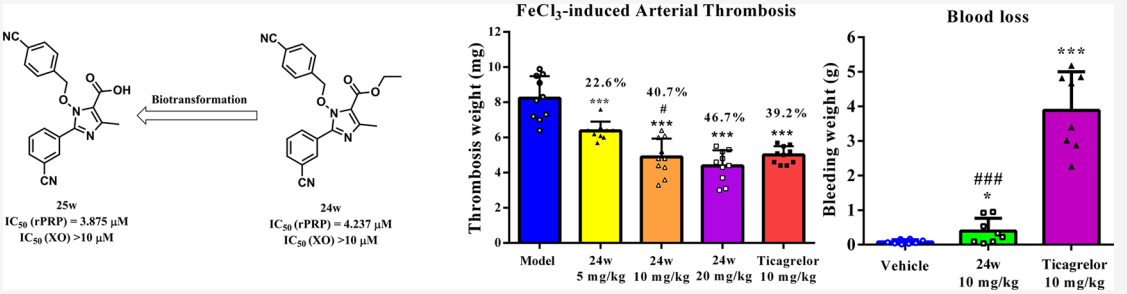

ABSTRACT: ADP-mediated platelet aggregation is signaled through G protein-coupled receptors $P2Y_1$ and $P2Y_{12}$ on the platelet. The clinical effectiveness of inhibiting $P2Y_{12}$ has been well established, and preclinical studies indicated that the inhibition of $P2Y_1$ could provide equivalent antithrombotic efficacy as $P2Y_{12}$ antagonists and reduce bleeding risks. On the basis of the 2-phenyl-1*H*-imidazole scaffold of our previously reported xanthine oxidase inhibitor **WSJ-557**, we first achieved the transition from the xanthine oxidase inhibitors to dual-target antagonists against $P2Y_1$ and $P2Y_{12}$. We described the structure−activity relationships of the 2-phenyl-1*H*-imidazole compounds, which led to the identification of the most potent antiplatelet agents, **24w** and **25w**, both showing a rapid onset of action in pharmacokinetic study. Furthermore, the rat model suggested that **24w** demonstrated a wider therapeutic window than ticagrelor, displaying equivalent and dose-dependent antithrombotic efficacy with lower blood loss compared to ticagrelor at same oral dose. These results supported that **24w** and **25w** could be promising drug candidates.

INRODUCTION

Acute coronary syndromes (ACSs), including unstable angina and acute myocardial infarction (AMI), are life-threatening thrombotic disorders, which have been the most common causes of morbidity and mortality over the past decade worldwide in cardiovascular patients.[1−3] Platelets display a major role in these thrombotic complications. They adhere to the subendothelial matrix following endothelial damage due to the rupture of an atherosclerotic plaque and then aggregate to cause thrombus formation.[4−] This activation process involves several platelet-activating agonists, such as adenosine diphosphate (ADP), thrombin, and thromboxane A_2.[6,7] Among them, ADP is a key mediator of activation as well as the aggregation of platelets. It could bind to two purinergic receptors $P2Y_1$ and $P2Y_{12}$, which both further activate glycoprotein IIb/IIIa on platelets and lead to sustained platelet aggregation as well as thrombus growth.[4−8] Specifically, $P2Y_{12}$ is mainly expressed on the membrane of human thrombocytes, and the binding of ADP to the $P2Y_{12}$ receptor results in a reduction of cAMP (cyclic adenosine monophosphate) levels, which is required to amplify and sustain the responses leading to a stable thrombus formation.[6,11−16] The inhibition of platelet aggregation targeting the $P2Y_{12}$ receptor has been recognized as an important element in the short-term treatment as well as for the long-term prevention of thrombotic events in patients with ACS.[2,11−14,16] $P2Y_1$ is ubiquitously expressed, and mobilizes the transitory increases in intracellular free Ca^{2+} ions leading to platelet shape changes in response to ADP.[16−19] It is reported that the inhibition of $P2Y_1$ could provide an equivalent antithrombotic efficacy to $P2Y_{12}$ in terms of blocking aggregation and reducing thrombus weight, whereas $P2Y_1$ antagonists may offer safety advantages in terms of a reduced bleeding liability.[18−21] This demonstrates that the $P2Y_1$ receptor could also represent a promising target for the development of new antiplatelet therapies.[18−21] Therefore,

Received: September 1, 2020

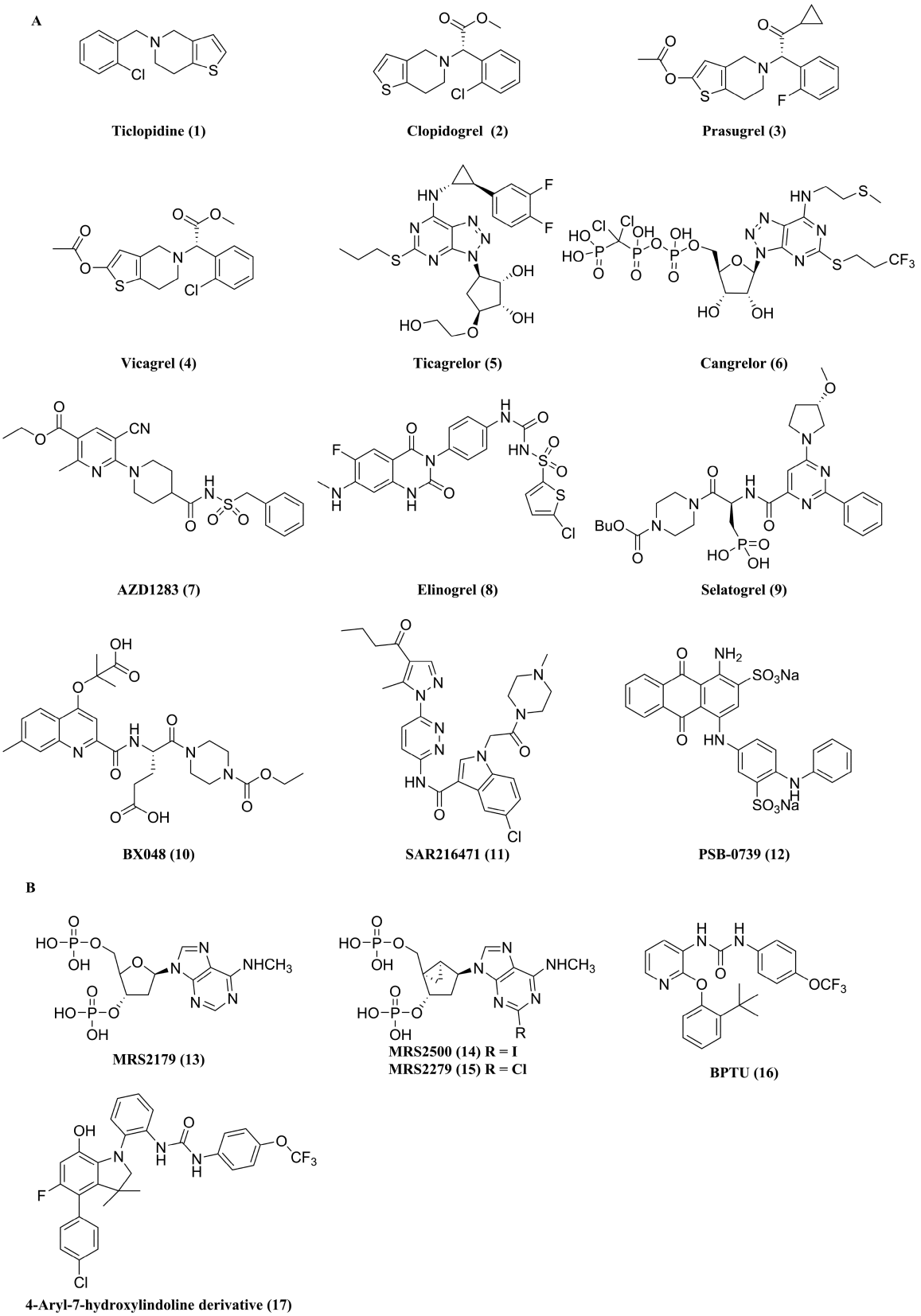

Figure 1. (A) Structures of $P2Y_{12}$ antagonists: ticlopidine (**1**), clopidogrel (**2**), prasugrel (**3**), vicagrel (**4**), ticagrelor (**5**), cangrelor (**6**), AZD1283 (**7**), elinogrel (**8**), selatogrel (**9**), BX048 (**10**), SAR216471 (**11**), and PSB-0739 (**12**). (B) Structures of $P2Y_1$ antagonists: MRS2179 (**13**), MRS2500 (**14**), MRS2279 (**15**), BPTU (**16**), and 4-aryl-7-hydroxylindoline derivative (**17**).

specifically inhibiting either of the two receptors or inhibiting both $P2Y_1$ and $P2Y_{12}$ could halt ADP-induced platelet aggregation for the treatment of arterial thrombosis and related diseases.[22−24]

https://dx.doi.org/10.1021/acs.jmedchem.0c01524
J. Med. Chem. XXXX, XXX, XXX−XXX

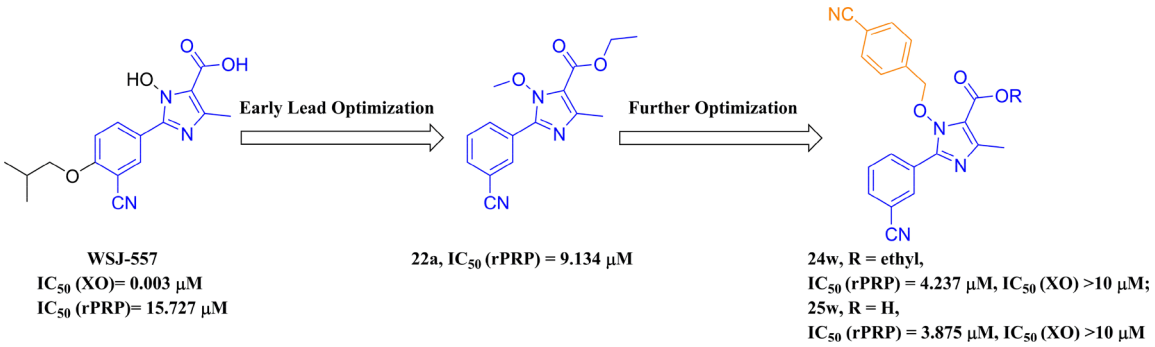

Figure 2. Design and structural modification of novel antiplatelet agents.

$P2Y_{12}$ receptor antagonists can be broadly classified into two classes on the basis of their chemical structures, namely, thienopyridines and nonthienopyridines.[16,25] The thienopyridine drugs, such as ticlopidine[16,25] (**1**, approved in 1978, Figure 1), clopidogrel[2,26] (**2**, approved in 1997, Figure 1), and prasugrel[27] (**3**, approved in 2009, Figure 1), are irreversible oral $P2Y_{12}$ receptor prodrugs and have proved to be successful in reducing the morbidity and mortality for cardiovascular patients.[2,16,28] In fact, the dual antiplatelet therapy of clopidogrel and acetylsalicylic acid has long been the gold standard of treatment.[16,29] However, they all require hepatic metabolic bioactivation for their active metabolites to covalently bind to the $P2Y_{12}$ receptor, which results in a slow onset of their pharmacological action.[2,16,30,31] This leads to the development of several reversible nonthienopyridine $P2Y_{12}$ receptor antagonists based on the nucleotide scaffold, such as ticagrelor[1] (**5**, approved in 2011, Figure 1) and cangrelor[30−32] (**6**, approved in 2015, Figure 1). Ticagrelor[1] (Figure 1) was the first drug developed and is administered orally. It reversibly binds the $P2Y_{12}$ receptor and has a faster onset of action than clopidogrel, but it has been shown to increase the rate of nonprocedure-related bleeding compared to clopidogrel.[33,34] Cangrelor[30−32] (Figure 1) is another nucleotide-derived reversible $P2Y_{12}$ antagonist with a rapid onset of action. However, it must be administered by a continuous intravenous infusion and is only used at the time of percutaneous coronary intervention (PCI) in patients not preloaded with an oral $P2Y_{12}$ receptor antagonist.[2,16] Consequently, there is still room for improvement in currently approved oral antiplatelet agents due to the drawbacks of slow onset of action and high bleeding risk.[14,16,35,36]

Recently, AZD1283[25,37,38] (**7**, Figure 1) and elinogrel[38,39] (**8**, Figure 1), based on the ethyl 6-aminonicotinate acyl sulfonamide and quinazoline-2,4-dione scaffolds, respectively, both showed potent antithrombotic efficacy and reduced bleeding effects in animal models.[11,40] Unfortunately, they were discontinued in clinical trials due to low metabolic stability and elevated liver transaminases.[11,39] Apart from these, other $P2Y_{12}$ receptor antagonists based on various chemical scaffolds, including BX048[41,42] (**10**, 7-methylquinoline-2-carboxamide derivative, Figure 1), SAR216471[43,44] (**11**, indole derivative, Figure 1), and PSB-0739[45,46] (**12**, anthraquinone derivative, Figure 1), are reported to exhibit more effective platelet inhibition, but they are still in preclinical research.[43−46] These facts indicate that the $P2Y_{12}$ antagonists distinct from the thienopyridine and nucleotide chemical scaffolds have received extensive attention and will hopefully minimize these disadvantages of currently available drugs.[16] Furthermore, two novel $P2Y_{12}$ receptor antagonists are currently in phase II clinical development: vicagrel[47] (**4**, Figure 1) and selatogrel[36,48] (**9**, Figure 1). Vicagrel (Figure 1), an irreversible thienopyridine oral $P2Y_{12}$ receptor antagonist, may show stronger platelet inhibition and a faster onset of action compared to clopidogrel. However, it still retains the same activation mechanism as prasugrel.[2,16,47] Selatogrel (2-phenylpyrimidine-4-carboxamide derivative, Figure 1) could be rapidly absorbed and shows a potentially lower risk of bleeding. However, it is only developed for subcutaneous not oral administration.[36,48] Besides, $P2Y_1$ antagonists, such as MRS2179[49] (**13**, Figure 1), MRS2500[20] (**14**, Figure 1), MRS2279[50] (**15**, Figure 1), BPTU[21] (**16**, Figure 1), and 4-aryl-7-hydroxylindoline derivative (**17**, Figure 1), are in preclinical development. Therefore, it is still necessary to explore an oral antiplatelet agent targeting $P2Y_1$ and $P2Y_{12}$ for the treatment of ACS on the basis of new chemical scaffolds to overcome the drawbacks of these clinical drugs and achieve a fast onset of action with less bleeding risk.[11,14,16,35,36]

In our previous reports of the nonpurine xanthine oxidase (XO) inhibitor, **WSJ-557** (2-(3-cyano-4-isobutoxyphenyl)-1-hydroxy-4-methyl-1*H*-imidazole-5-carboxylic acid, Figure 2) demonstrated a stronger XO inhibitory potency (IC_{50} = 0.003 μM for XO) than that of febuxostat (IC_{50} = 0.01 μM for XO).[51,52] The remarkable XO inhibitory potency of **WSJ-557** encouraged us to investigate its pharmacokinetic (PK) profiles to further assess its development potential.[52] In this procedure, it was found that **WSJ-557** could delay blood coagulation, which drove us to investigate its action mechanism. The subsequent antiplatelet aggregation assay induced by ADP showed that the compound could display an apparent antiplatelet potency (IC_{50} = 15.727 μM).

These interesting results suggested that the **WSJ-557** with a 2-phenyl-1*H*-imidazole scaffold could be considered as an initial compound for the development of $P2Y_1$ and $P2Y_{12}$ dual antagonists.

We described the procedure for switching the XO inhibitor **WSJ-557** to dual-target antagonists of $P2Y_1$ and $P2Y_{12}$ through structure−activity relationships (SAR) investigation of the 2-phenyl-1*H*-imidazole compounds, which led to the identification of compounds **24w** and **25w** as the most potential antiplatelet agents in ADP-induced rabbit platelet-rich plasma (rPRP) aggregation test *in vitro* (Figure 2). $P2Y_1$ and $P2Y_{12}$ binding assays were also performed to investigate the effect of compound **25w** on platelet $P2Y_1$ and $P2Y_{12}$ receptors by the flow cytometric assay. Moreover, the probable binding models of the target compounds **24w** and **25w** with $P2Y_1$ and $P2Y_{12}$ receptors were explored by molecular modeling. Additionally, metabolic stability, pharmacokinetic profile, and acute toxicity studies were performed to support the pharmacological

https://dx.doi.org/10.1021/acs.jmedchem.0c01524
J. Med. Chem. XXXX, XXX, XXX−XXX

Scheme 1[a]

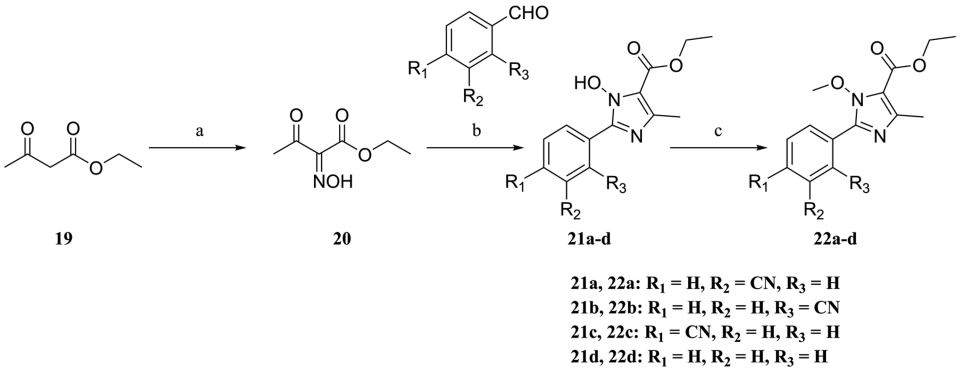

[a]Reagents and conditions: (a) $NaNO_2$, CH_3COOH, 0−5 °C; (b) Benzaldehyde derivatives, CH_3COOH/CH_3COONH_4, 50 °C; (c) Me_2SO_4, K_2CO_3, DMF, 0 °C.

Scheme 2[a]

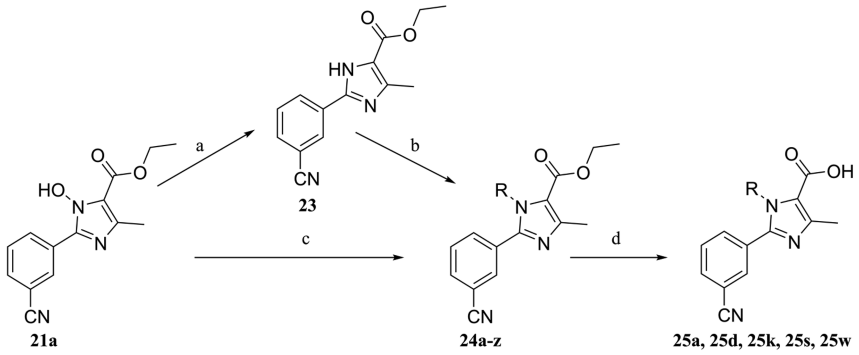

24a: R = methyl	24k: R = benzyloxyl	24u: R = [4-(methoxycarbonyl)benzyl]oxyl
24b: R = isopropyl	24l: R = (2-fluorobenzyl)oxyl	24v: R = (4-nitrobenzyl)oxyl
24c: R = isopropoxyl	24m: R = (3-fluorobenzyl)oxyl	24w: R = (4-cyanobenzyl)oxyl
24d: R = allyloxyl	24n: R = (4-fluorobenzyl)oxyl	24x: R = (2-cyanobenzyl)oxyl
24e: R = 2-ethoxyethoxyl	24o: R = (2-chlorobenzyl)oxyl	24y: R = (3-cyanobenzyl) oxyl
24f: R= 2-ethoxy-2-oxoethoxyl	24p: R = (3-chlorobenzyl)oxyl	25a: R = methoxyl
24g: R = 3-hydroxypropoxyl	24q: R = (4-chlorobenzyl)oxyl	25d: R = allyloxyl
24h: R = 2-amino-2-oxoethoxyl	24r: R = (4-bromobenzyl)oxyl	25k: R = benzyloxyl
24i: R = 2-carboxyethoxyl	24s: R = (4-methylbenzyl)oxyl	25s: R = (4-methylbenzyl)oxyl
24j: R = pyridin-4-ylmethoxyl	24t: R = (4- methoxybenzyl)oxyl	25w: R = (4-cyanobenzyl)oxyl

[a]Reagents and conditions: (a) Me_3SiCl, NaI, CH_3CN, reflux; (b) Me_2SO_4, K_2CO_3, DMF, 0 °C; (c) RX, K_2CO_3, KI, N_2, DMF, 0−50 °C; (d) LiOH, THF, H_2O, 50 °C.

characterization of the most potent compounds **24w** and **25w**. Lastly, the compound **24w** was further evaluated in a rat ferric chloride model as well as a rat-tail-bleeding model to investigate its antithrombotic effect and bleeding risk, respectively. These results obtained from the investigations supported that **24w** and **25w** could be promising drug candidates for the treatment of arterial thrombosis and related diseases.

RESULTS AND DISCUSSION

Chemistry. The key intermediate ethyl 2-hydroxyimino-3-oxobutanoate **20** was obtained by nitrosation of the commercially available ethyl 3-oxobutanoate **19** with sodium nitrite in acetic acid.[51] Commercially available benzaldehyde derivatives were cyclized with the key intermediate **20** to give compounds **21a−d**, which were further alkylated with iodomethane in *N*,*N*-dimethylformamide in the presence of anhydrous potassium carbonate to provide target compounds **22a−d** (Scheme 1).[51]

Then, the 1-hydroxyl moiety of compound **21a** was removed with chlorotrimethylsilane and sodium iodide by refluxing in acetonitrile to provide compound **23**,[53] which was further alkylated with iodomethane or 1-bromo-2-methylpropane in *N*,*N*-dimethylformamide in the presence of anhydrous potassium carbonate and potassium iodide to provide compounds **24a** and **24b**.[51] Compounds **24c−y** were prepared through the alkylation reaction of the compound **21a** with appropriate alkyl halides in DMF in the presence of K_2CO_3 and KI, which were hydrolyzed using an aqueous solution of lithium hydroxide to afford the compounds **25a**, **25d**, **25k**, **25s**, and **25w** (Scheme 2).[51] The structures were elucidated by high-resolution mass spectrometry (HRMS), infared (IR), proton nuclear magnetic resonance (^{1}H NMR), and ^{13}C NMR spectra (Supporting Information). All spectral data were in accordance with the assumed structures.

Discovery of Lead Compound 22a. Since the ethyl ester of **WSJ-557** (compound **18**) displays an equivalent antiplatelet potency (IC_{50} = 16.825 μM), the ethyl ester group of 5-position was retained for further structural optimization for the

https://dx.doi.org/10.1021/acs.jmedchem.0c01524
J. Med. Chem. XXXX, XXX, XXX−XXX

possibility of higher bioavailability. Initially, we found that removing the 4′-isobutoxy group had no apparent effect on its antiplatelet potency (**21a** vs **18**, IC_{50} = 17.636 and 16.825 μM, respectively, Table 1). In addition, the introduction of a small

Table 1. *In Vitro* Antiplatelet Aggregation Potency of Lead Optimization on Imidazole Derivatives

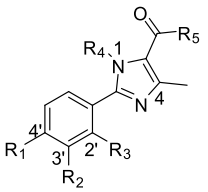

Compounds	R_1	R_2	R_3	R_4	R_5	IC_{50}[a] (μM)
WSJ-557		-CN	-	-OH	-OH	15.727 ± 0.481
18		-CN	-	-OH	-OEt	16.825 ± 0.874
21a	-	-CN	-	-OH	-OEt	17.636 ± 0.952
22a	-	-CN	-	$-OCH_3$	-OEt	9.134 ± 0.346
22b	-	-	-CN	$-OCH_3$	-OEt	14.857 ± 0.0568
22c	-CN	-	-	$-OCH_3$	-OEt	13.353 ± 1.035
22d	-	-	-	$-OCH_3$	-OEt	> 30
23	-	-CN	-	-	-OEt	> 30

[a]ADP-induced platelet aggregation ([ADP] = 2.27 μM, n = 3), rabbit platelet-rich plasma (rPRP).

hydrophobic methyl group into the 1-hydroxy position of imidazole moiety was beneficial for remarkably increasing the antiplatelet potency (**21a** < **22a**, IC_{50} = 17.636 and 9.134 μM, respectively). Consequently, **22a** was further examined to determine the antiplatelet influence by cyano group positions on the phenyl moiety. The corresponding *ortho*-, *para*-, and no cyano substituted derivatives were synthesized, and these compounds showed a marked decrease in inhibitory potency (**22b**, **22c**, and **22d** vs **22a**, IC_{50} = 14.857, 13.353, > 30, and 9.134 μM, respectively), which implied that *meta*-cyano substitution was necessary for the antiplatelet potency. Moreover, removing the 1-hydroxy group led to compound **23**, which displayed a loss in antiplatelet potency (**23**, IC_{50} > 30 μM). Therefore, on the basis of these data, the potent lead compound **22a** containing the 2-phenyl-1*H*-imidazole scaffold was selected for further optimization.

Identification of Compounds 24w and 25w. The observation that introducing a methyl at the hydroxyl group at the 1-position could increase the antiplatelet potency greatly inspired us to investigate the substitution pattern at the 1-position further. First, the compounds containing methyl, isopropyl, and isopropoxy groups were synthesized. The results suggested that the antiplatelet potency of inserting alkoxy groups into the 1-position was stronger than those of corresponding alkyl groups (**24a** < **22a**, **24b** < **24c**, IC_{50} = 22.136, 9.134, 9.259, and 6.736 μM, respectively, Table 2). Then, introducing allyloxy, ethoxyethoxy, and 2-ethoxy-2-oxoethoxy groups at the 1-position led to compounds **24d**, **24e**, and **24f**, and their antiplatelet potency was further enhanced (**24d**, **24e**, and **24f** vs **22a**, IC_{50} = 5.856, 6.247, 6.796, and 9.134 μM, respectively). For comparison, the more polar compounds **24g**, **24h**, and **24i** containing hydroxypropoxy, 2-amino-2-oxoethoxy, and 2-carboxyethyloxy groups at the 1-position were synthesized, and the results showed that compound **24g** exhibited an IC_{50} value of 11.352 μM and the antiplatelet potency for compounds **24h** and **24i** disappeared completely. This indicated that enhancing the polarity of substituents at the 1-position was not beneficial for antiplatelet potency.

In order to explore the antiplatelet effect of alkoxy groups at the 1-position further, the pyridin-4-ylmethoxy and benzloxy substitutions were introduced to provide compounds **24j** and **24k**, and they exhibited an apparent inhibitory potency in the platelet aggregation assay than that of compound **22a** (**24j**, **24k** vs **22a**, IC_{50} = 6.196, 5.934, and 9.134 μM, respectively). The remarkable antiplatelet potency of compound **24k** encouraged us to tune the substituents on the phenyl moiety. First, the electron withdrawing substituents, such as fluoro and chloro substituents, were inserted at *ortho*, *meta*, and *para* positions of the benzyloxy group. Among them, the *para*-substituted derivatives showed a better antiplatelet aggregation potency compared to *ortho*- and *meta*-substituted derivatives (**24n** > **24l** > **24m**; **24q** > **24o** > **24p**, IC_{50} = 5.879, 8.987, 22.358, 6.825, 8.705, and 19.357 μM, respectively), These results showed that the insertion of fluoro and chloro atoms at the *para* position was beneficial for improving the inhibitory potency. Consequently, the continued investigations of substituents at the *para* position of the benzyloxy group were carried out. The introduction of bromo, methyl, methoxy, methoxycarbonyl, nitro, and cyano groups into the *para* position led to compounds **24r**−**y** with IC_{50} values of 24.590, 6.311, 6.826, 9.466, 8.754, and 4.237 μM, respectively. To our surprise, compound **24w** (IC_{50} = 4.237 μM) with a cyano group at the *para* position displayed the most remarkable inhibitory potency, and it was comparable to that of ticagrelor (IC_{50} = 7.213 μM). Subsequently, the corresponding *ortho* and *meta* counterparts were examined. The results showed that **24x** displayed a 2.2-fold decrease in inhibitory potency in comparison to compound **24w**, and the inhibitory potency of compound **24y** was lost (**24w** and **24y**, IC_{50} = 9.376 and >30 μM, respectively). This showed the same inhibitory tendency as compounds with fluoro and chloro atoms substituted at benzyloxy moiety. Presumably, the cyano group substituted at the *para* position kept the 4-cyanobenzyloxy moiety in a more favorable position so that it could form better interactions with amino acid residues at the active pocket.

Lastly, to explore the inhibitory potency of the corresponding acids, compounds **22a**, **24d**, **24k**, **24s**, and **24w** were hydrolyzed to obtain compounds **25a**, **25d**, **25k**, **25s**, and **25w**, and the compounds showed equal potency in comparison to their ester counterparts. (**25a** vs **24a**; **25d** vs **24d**; **25k** vs **24k**; **25s** vs **24s**, IC_{50} = 7.987 vs 9.134 μM; IC_{50} = 6.350 vs 5.856 μM; IC_{50} = 6.238 vs 5.934 μM; IC_{50} = 6.563 vs 6.311 μM, respectively). Among them, compound **25w** (IC_{50} = 3.875 μM), the acid of compound **24w**, displayed the same remarkable inhibitory potency as that of compound **24w**, and it was also comparable to that of ticagrelor (IC_{50} = 7.213 μM).

$P2Y_1$-Mediated Cytosolic Ca^{2+} Increases Assay. ADP activates platelets by simultaneously acting on two platelet G protein−coupled receptors $P2Y_1$ and $P2Y_{12}$.[18] However, it is not clear which of the two receptors was inhibited by the test

https://dx.doi.org/10.1021/acs.jmedchem.0c01524
J. Med. Chem. XXXX, XXX, XXX−XXX

Table 2. *In Vitro* Antiplatelet Aggregation Potency of Variations Around the Imidazole Moiety

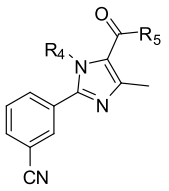

Compounds	R_4	R_5	IC_{50} [a] (μM)	Compounds	R_4	R_5	IC_{50} [a] (μM)
24a	-CH_3	-OEt	22.136 ± 0.703	**24q**	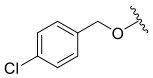	-OEt	6.825 ± 0.265
24b		-OEt	9.259 ± 0.499	**24r**	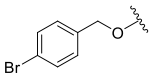	-OEt	24.590 ± 0.895
24c		-OEt	6.736 ± 0.326	**24s**	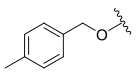	-OEt	6.311 ± 0.399
24d	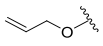	-OEt	5.856 ± 0.0165	**24t**	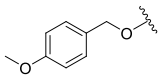	-OEt	6.826 ± 0.0856
24e	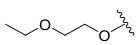	-OEt	6.247 ± 0.210	**24u**	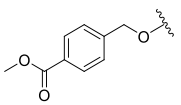	-OEt	9.466 ± 0.856
24f	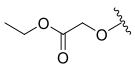	-OEt	6.796 ± 0.152	**24v**	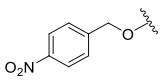	-OEt	8.754 ± 0.159
24g	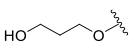	-OEt	11.352 ± 0.213	**24w**	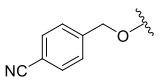	-OEt	4.237 ± 0.0156
24h	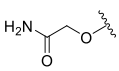	-OEt	> 30	**24x**	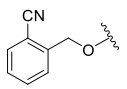	-OEt	9.376 ± 0.565
24i	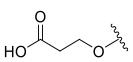	-OEt	> 30	**24y**	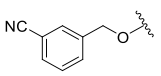	-OEt	> 30
24j	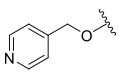	-OEt	6.196 ± 0.0526	**25a**	-OCH_3	OH	7.987 ± 0.217
24k	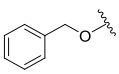	-OEt	5.934 ± 0.285	**25d**	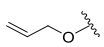	OH	6.350 ± 0.469
24l	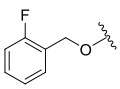	-OEt	8.987 ± 0.443	**25k**	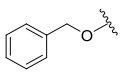	OH	6.238 ± 0.324
24m	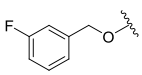	-OEt	22.358 ± 1.358	**25s**	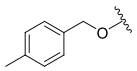	OH	6.563 ± 0.357
24n	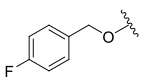	-OEt	5.879 ± 0.196	**25w**	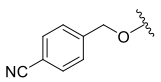	OH	3.875 ± 0.269
24o	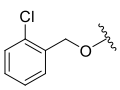	-OEt	8.705 ± 0.242	**Ticagrelor**	-	-	7.213 ± 0.251
24p	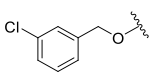	-OEt	19.357 ± 0.355	**BPTU**	-	-	5.537 ± 0.619

[a]ADP-induced platelet aggregation ([ADP] = 2.27 μM, n = 3), rabbit platelet-rich plasma (rPRP).

https://dx.doi.org/10.1021/acs.jmedchem.0c01524
J. Med. Chem. XXXX, XXX, XXX−XXX

compounds to exert their antiplatelet effect. To elucidate the action mechanism of these test compounds in its antiplatelet potency, the antagonist effects of the most potent compound **25w** on platelet $P2Y_1$ were determined by measuring the $P2Y_1$-mediated cytosolic Ca^{2+} increase from intraplatelet stores after stimulation by ADP as previously described with minor modifications.[22,23,46,54,55] The results are listed in Table 3.

Table 3. Inhibitory Potency of ADP-Induced Ca^{2+} Increase

compounds	inhibition of Ca^{2+} rise in platelets (IC_{50}, μM)[a]
25w	2.59 ± 0.36
BPTU	3.03 ± 0.63

[a]In diluted rPRP, n = 3.

Compound **25w** displayed a potent inhibitory effect against $P2Y_1$ on platelet with an IC_{50} value of 2.59 μM, which was comparable to that of **BPTU** (IC_{50} = 3.03 ± 0.63 μM), suggesting that compound **25w** exerted its antiplatelet potency mainly by inhibiting receptor $P2Y_1$ on platelet. Besides, several research studies have already demonstrated that the $P2Y_1$ antagonists could have an equivalent antithrombotic efficacy but less bleeding compared with the $P2Y_{12}$ antagonist clopidogrel.[19,20] Therefore, this activity evaluation of $P2Y_1$ rationalized that compound **24w** (parent compound **25w** released from prodrug **24w** in rats after oral administration) exhibited a therapeutically equivalent antithrombotic effect as that of ticagrelor at the same oral dose, with remarkably less blood loss than ticagrelor.

$P2Y_{12}$ Binding Assay. To examine the effect of compound **25w** on the platelet $P2Y_{12}$ receptor in response to ADP (no test of compound **24w** due to poor solubility), $P2Y_{12}$ binding assay was performed by measuring the $P2Y_{12}$-mediated decrease in intraplatelet phosphorylated vasodilator-stimulated phosphoprotein (VASP) using a flow cytometric PLT VASP/$P2Y_{12}$ kit (Biocytex, Marseille, France).[22,23,56−59] ADP, as an agonist, activated the $P2Y_{12}$ receptor to trigger the reaction of VASP phosphorylation. Meanwhile, it also antagonized the $P2Y_{12}$ receptor to induce the decrease of VASP phosphorylation. Then, the test compounds were added to antagonize the $P2Y_{12}$ receptor to attenuate the antagonistic effect of ADP, resulting in the increase of VASP phosphorylation, and this protocol was used to measure the antagonistic effect of compounds.[56−59] Thus, the percentage inhibition of prostaglandin E_1 (PGE_1)-stimulated VASP phosphorylation was set as 100%, and no stimulation was set as 0% inhibition.[59] Specifically, the percentage inhibition was calculated relative to vehicle (0% inhibition) and PGE_1 (100% inhibition): inhibition (%) = $[(MFI_{(PGE1)} - MFI_{(PGE1+ADP+compound)})/(MFI_{(PGE1)} - MFI_{(negative)})] \times 100$,[60] where MFI is the mean fluorescence intensity of VASP phosphorylation.[59] In the absence of ADP, $P2Y_{12}$−VASP phosphorylation was performed to investigate whether compounds possessed an agonistic effect on the $P2Y_{12}$ receptor.

As expected, PGE_1 is added to induce the full phosphorylation of VASP, which was set as 100%, and VASP phosphorylation in the presence of the $P2Y_{12}$ agonist ADP (3 μM) was significantly reduced in comparison with PGE_1 alone (Figure 3).[22,23] Furthermore, compound **25w** and ticagrelor both were able to dose dependently antagonize the ADP-induced reduction of VASP phosphorylation compared to PGE_1 alone, indicating that the antagonist effects of compound **25w** and ticagrelor were mediated through

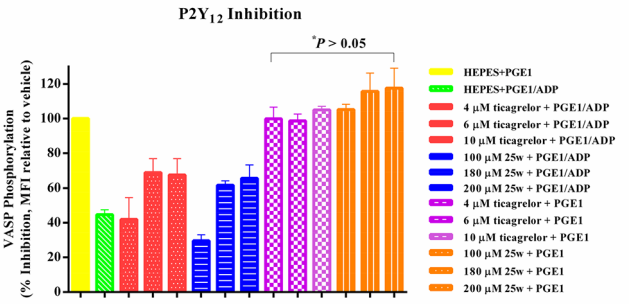

Figure 3. Inhibition of ADP-induced, $P2Y_{12}$-mediated decrease in VASP phosphorylation by compound **25w** or ticagrelor. PGE_1-stimulated VASP phosphorylation and its attenuation by ADP in the presence and absence of the test compounds were measured by flow cytometry. The data were reported as the mean ± SD (n = 3; *P > 0.05, as compared to PGE_1 alone).

specifically binding to $P2Y_{12}$. Among them, the antagonist potency of compound **25w** was higher than that of MRS2395, an antagonist for the $P2Y_{12}$ purinoceptor reported in the literature.[61] Nevertheless, the antagonist potency of both compound **25w** and MRS2395 was lower than that of ticagrelor (**ticagrelor** > **25w** > **MRS2395**, IC_{50} = 5.14, 148.92, and 176−196 μM, respectively). In addition, compound **25w** and ticagrelor both could not cause a decrease of VASP phosphorylation in the absence of ADP, which was comparable to that of PGE_1 alone, suggesting that they did not possess $P2Y_{12}$ agonistic effects.[22,23] The results above proved that compound **25w** could bind to $P2Y_{12}$ purinoceptor as an antagonist. Therefore, we could confirm that compound **25w** exerted its antiplatelet effect through both $P2Y_1$ and $P2Y_{12}$ receptors.

Xanthine Oxidase Inhibitory Activity. The evaluation of the *in vitro* bovine XO inhibitory potency of compounds **24w** and **25w** was performed with febuxostat as a reference compound. The results showed that compounds **24w** and **25w** displayed no significant inhibition against XO (not active, inhibition at 10 μM < 50%), and the IC_{50} value of febuxostat was 0.0189 μM.

Docking Studies. To explore a probable interaction model of compounds **24w** and **25w** with $P2Y_1$ and $P2Y_{12}$, the molecular docking of compounds **24w** and **25w** in **MRS2500** and **AZD1283** binding pockets of proteins was performed using the Glide XP docking protocol (2016, Schrodinger Suite).[62] The X-ray crystal structures of the $P2Y_1$/MRS2500 (PDB: 4XNW)[63] and $P2Y_{12}$/AZD1283 (PDB: 4NTJ)[64] used in the docking studies were obtained from the RCSB Protein Data Bank, and **MRS2500** as well as **AZD1283** were adopted as references. The proteins were prepared by removing all water molecules and adding all hydrogen atoms using Protein Preparation Wizard (2016, Schrodinger Suite).[62] The phosphonic acid and carboxyl groups of all compounds were calculated in dissociated forms using the LIGPREP module (2016, Schrodinger Suite).[62]

The binding models of compounds **24w** and **25w** were illustrated by Pymol[65] (Figure 4). For the binding mode of $P2Y_1$, we found that the carboxylic acid group of compound **25w** could engage in three hydrogen bonds with key residues Thr205, Tyr206, and Arg310, which was almost equivalent to the interactions formed by the phosphate group of **MRS2500**, and it could also interact with key residue Asn283 *via* two hydrogen bonds. In addition, an extra electrostatic interaction

https://dx.doi.org/10.1021/acs.jmedchem.0c01524
J. Med. Chem. XXXX, XXX, XXX−XXX

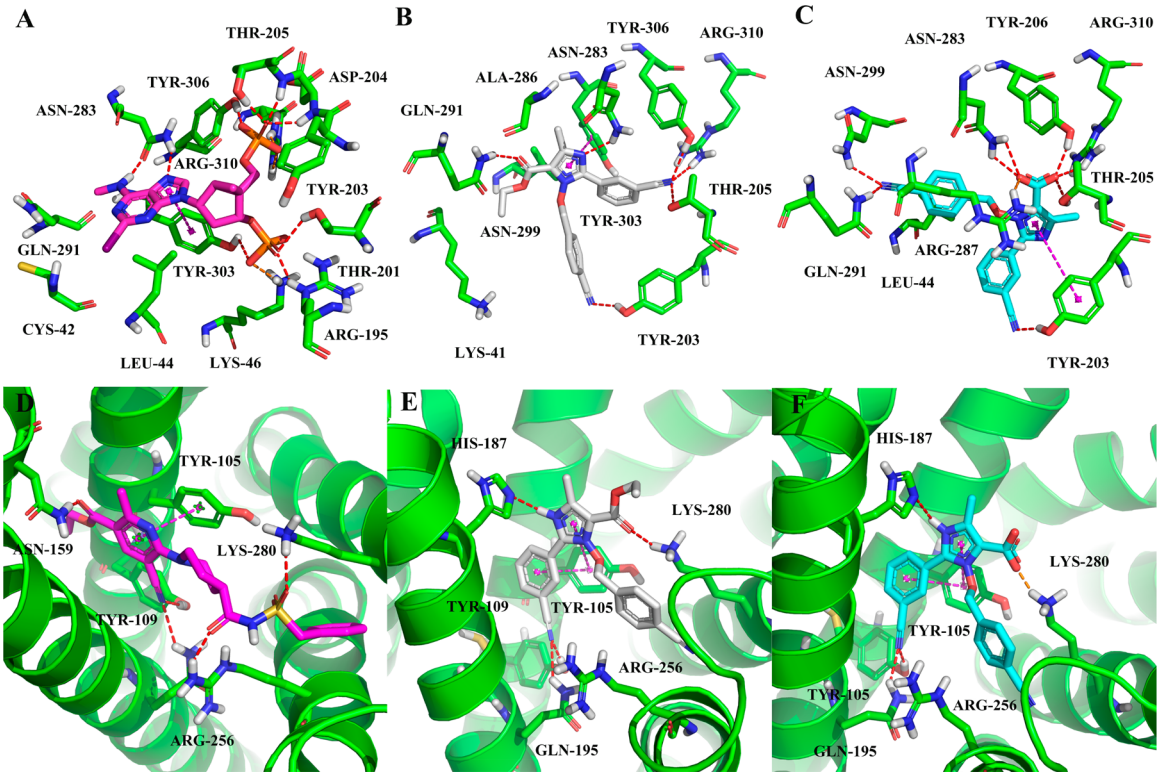

Figure 4. Binding modes of (A) **MRS2500**, (B) compound **24w**, and (C) compound **25w** in the $P2Y_1$ receptor (PDB: 4XNW). Binding modes of (D) **AZD-1283**, (E) compound **24w**, and (F) **25w** in the $P2Y_{12}$ receptor (PDB: 4NTJ). Protein is shown as a cartoon, and small molecules are shown as sticks. Hydrogen bonds, $\pi-\pi$ stacking interactions, and electrostatic interaction are depicted by red, purple, and orange dashed lines, respectively. Residues of $P2Y_1$ and $P2Y_{12}$ interacting with inhibitors are depicted by green sticks.

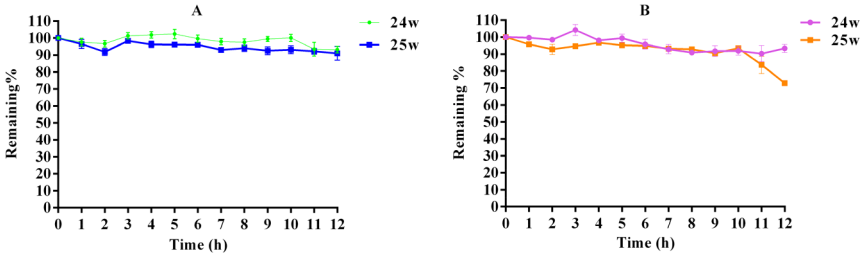

Figure 5. (A and B) Stability profiles of compounds **24w** and **25w** in simulated gastric and intestinal fluids. Each value is the mean ± SEM; $n = 3$.

was formed between **25w** and Arg287 (Figure 4C), and a $\pi-\pi$ stacking interaction was observed between the imidazole moiety of **25w** and Tyr203. Moreover, the cyano groups on phenyl and benzyl moieties of **25w** formed new hydrogen bonds with Tyr203, Gln291, and Asn299, respectively, which was lacking in **MRS2500**. In terms of compound **24w**, the similar key hydrogen bonds with Thr205, Tyr206, Arg310, and Asn283 were also observed at the cyano group on the phenyl moiety and the N atom on the imidazole ring, and the cyano and ester carbonyl groups were able to interact with Tyr203 and Gln291 *via* two hydrogen bonds. The imidazole moiety of compound **24w** could also interact with Tyr 303 through a $\pi-\pi$ stacking interaction. Nevertheless, compounds **24w** and **25w** both lacked hydrogen bonds formed by the other phosphate group of **MRS2500** with Lys46, Arg195, Thr201, Tyr203, and Tyr303.

The docking results of $P2Y_{12}$ showed that the cyano groups of compounds **24w** and **25w** were able to form two hydrogen bonds with the side chains of key residues Tyr109 and Gln195 (Figure 4B,C), which was in agreement with the binding mode of the cyano group of **AZD1283** in the binding pocket of $P2Y_{12}$ (Figure 4A). Moreover, the negatively charged carboxylic acid group of compound **25w** formed an electrostatic interaction with the positively charged side chain of Lys280, which is consistent with those observed in acidic groups such as sulfonate or carboxylic acid groups presented in anthraquinone and glutamic acid piperazine $P2Y_{12}$ antagonists,[66] whereas the ester carbonyl group of compound **24w** only engaged in a hydrogen bond with the side chain of Lys280. Meanwhile, the phenyl ring of compounds **24w** and **25w** occupied the same region as the pyridine moiety of AZD1283 through an aromatic $\pi-\pi$ stacking interaction with Tyr105. Moreover, compared to AZD1283, the imidazole ring of compounds **24w** and **25w** formed an additional aromatic $\pi-\pi$ stacking interaction with Tyr105, and the 4-cyanobenzyl group further inserted into the cavity occupied by the piperidine moiety of AZD1283.

Simulated Gastric and Intestinal Fluid Stability. To characterize the *in vitro* metabolic stability of compounds **24w** and **25w**, they were incubated with simulated gastric and

https://dx.doi.org/10.1021/acs.jmedchem.0c01524
J. Med. Chem. XXXX, XXX, XXX−XXX

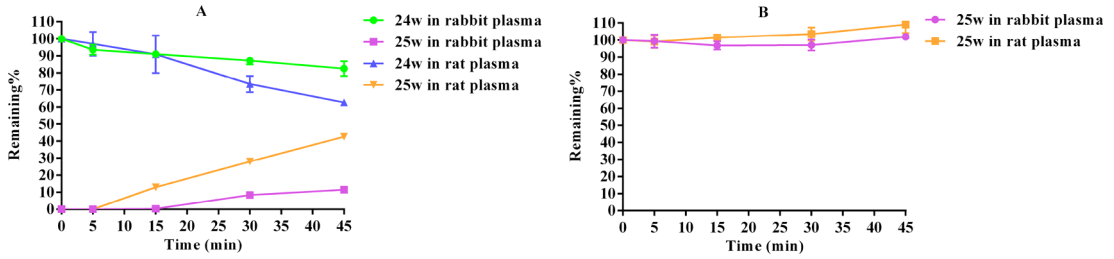

Figure 6. Stability and metabolism profiles of compounds (A) **24w** and (B) **25w** in rabbit and rat plasma. Each value is the mean ± SEM; $n = 3$.

intestinal fluid, and the remaining percentages of compounds **24w** and **25w** after incubation are summarized in Figure 5. After a 12 h incubation period in simulated gastric fluid, approximately 90% of the parent compounds **24w** and **25w** remained intact, which suggested that they were considerably stable in simulated gastric fluid. After a 12 h incubation period in simulated intestinal fluid, compound **24w** was also stable with about 93% remaining while compound **25w** was moderately stable in simulated intestinal fluid, due to 73% of its parent compound left. These results suggested that compounds **24w** and **25w** should be stable in stomach and intestine.

Stability Studies in Plasma. The *in vitro* stability profiles of compounds **24w** and **25w** were further studied by incubation with both rabbit and rat plasma to observe the disappearance of the prototype and formation of the metabolite. Figure 6 showed that 12% of compound **24w** was converted to compound **25w** by 45 min in rabbit plasma. Meanwhile, in rat plasma, 43% of the compound **24w** was hydrolyzed to compound **25w** by 45 min. These results suggested that compound **24w** could be rapidly converted to compound **25w** in plasma, which is consistent with the later PK studies in rats after the oral administration of **24w**. The hydrolysis rate of compound **24w** in rat plasma was greater than that in rabbit plasma. Moreover, no significant degradation of compound **25w** was observed in these two media during the incubation period, which indicated that compound **25w** was rather stable in both rabbit and rat plasma, and compound **24w** could be used as a prodrug of **25w**.

Metabolic Stability in Liver Microsomes. The hepatic metabolism plays a vital role in biotransformation in the majority of prodrugs, and liver microsomal metabolic stability is widely used in the research of drug metabolism.[67] Therefore, compounds **24w** and **25w** were further evaluated for their *in vitro* liver microsomal metabolic stability, and the data are listed in Table 4. In Figure 7A,C, compound **24w** was rapidly converted to compound **25w** in both rat liver microsomes (RLMs) and human liver microsomes (HLMs), which indicated that compound **24w** could be rapidly converted into compound **25w** by hepatic metabolism and further confirmed the formation of compound **25w** in later PK studies in rats after the oral administration of **24w**. Moreover, the liver microsomal stability of compound **24w** in HLMs ($t_{1/2}$ = 120.65 min, Figure 7C) was better in that in RLMs ($t_{1/2}$ = 23.13 min, Figure 7A), suggesting that there was a species difference of compound **24w** in both RLMs and HLMs, and compound **24w** could be converted to compound **25w** rapidly in rat liver. In addition, compound **25w** ($t_{1/2}$ > 120 min in both RLMs and HLMs) was considerably stable in both RLMs and HLMs (Figure 7B,D).

Table 4. Microsomal Stability of Compounds 24w and 25w[a]

compound	species	$t_{1/2}$[b] (min)	Cl_{int}[c] (mL/min/mg protein)
24w	rat	23.13	0.060
	human	120.65	0.011
25w	rat	>120	
	human	>120	

[a]Microsomal protein (0.50 mg/mL), NADPH-regenerating system, [inhibitor], 0.2 μM; incubation at 37 °C. [b]$T_{1/2}$: elimination half-life. [c]Cl_{int}: intrinsic body clearance.

CYP450 Inhibition Assay. CYP450-mediated drug−drug interaction is one of the important reasons for the dropout of drug candidates during new drug development.[68] Therefore, testing for drug−drug interaction potential of new chemical entities is essential for developing a novel drug.[68−70] As a result, compounds **24w** and **25w** were selected to further evaluate their *in vitro* inhibitory potential of major CYP450 enzymes including CYP1A2, CYP2A6, CYP2C9, CYP2C19, CYP2D6, CYP2E1, and CYP3A4 in a CYP450 inhibition cocktail assay, and the results are summarized in Table 5. Indeed, compound **25w** was found to show no significant inhibition against these CYP450 isoforms at 10 μM, which indicated that its IC_{50} value against these major CYP450 isoforms was greater than 10 μM. This result implied that compound **25w** showed no apparent drug−drug interaction potential at 10 μM. However, compound **24w** exhibited a weak inhibitory potency against CYP2D6 with an inhibition of 31.69% at 10 μM, suggesting that there might be low liability for drug−drug interactions between **24w** and CYP2D6.

Pharmacokinetic Studies. To explore the pharmacokinetic assessment of compounds **24w** and **25w**, they were further evaluated for their PK properties in Sprague-Dawley rats, as shown in Figure 8, and their noncompartmental PK parameters are listed in Table 6.

For a single oral administration of **24w** (10 mg/kg), the prototype of compound **24w** (below analytical detection limit of quantification: 10 ng/mL) was not observed in the beginning of the oral administration, while compound **25w** was immediately detected at 10 min after the oral administration of **24w** (Figure 8). This suggested that the compound **24w** could be rapidly converted into the metabolite **25w**, and these results were consistent with *in vitro* plasma and liver microsomal stability. Furthermore, the average time for compounds **24w** and **25w** to reach the maximum concentration (T_{max}) was shorter than that of ticagrelor[36] (ticagrelor > **24w** > **25w**, T_{max} = 4 > 0.46 > 0.167 h, respectively), indicating that they both were absorbed quickly into circulation. This might demonstrate a faster onset of action than current clinical oral $P2Y_{12}$ antagonists.[14,16,35,36] Meanwhile, the half-lives ($t_{1/2}$) of compounds **24w** and **25w** were both 13 h, suggesting that they both could achieve a longer duration of action. Among

https://dx.doi.org/10.1021/acs.jmedchem.0c01524
J. Med. Chem. XXXX, XXX, XXX−XXX

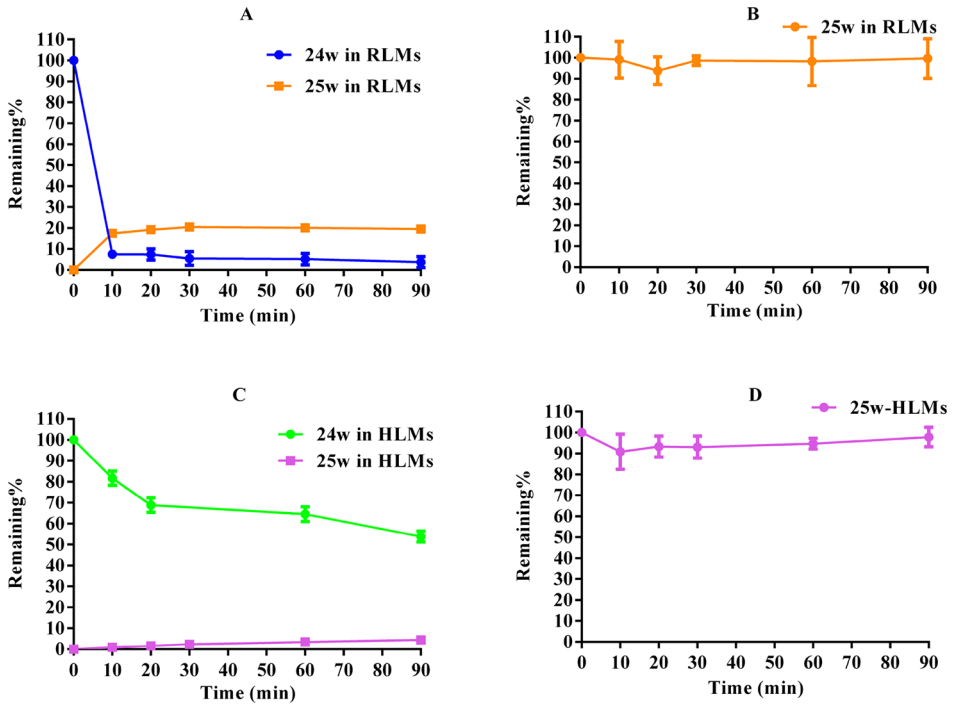

Figure 7. Stability profiles of compounds **24w** and **25w** obtained in both RLMs and HLMs: (A) incubation of **24w** in RLMs; (B) incubation of **25w** in RLMs; (C) incubation of **24w** in HLMs; (D) incubation of **25w** in HLMs. The data represent the mean ± SEM of three independent experiments (n = 3).

Table 5. CYP450 Inhibition of Compounds 24w and 25w

	inhibition at 10 μM (%)						
compounds	CYP1A2[a]	CYP2A6[b]	CYP2C9[c]	CYP2C19[d]	CYP2D6[e]	CYP2E1[f]	CYP3A4[g]
24w	3.85	7.69	0.024	4.52	31.69	8.68	2.16
25w	0.11	3.64	0.41	1.97	2.42	6.79	7.40

[a]Phenacetin. [b]Coumarin. [c]Tolbutamide. [d]S-Mephenytoin. [e]Dextromethorphan, [f]Chlorzoxazone. [g]Nifedipine.

them, compound **24w** displayed slightly better PK properties compared to those of **25w**, including higher plasma exposure ($AUC_{0-\infty}$ = 1135.08 ng·h/mL) and moderate oral bioavailability (F = 32.4%). On the basis of its favorable pharmacokinetic profiles, compound **24w** was selected for further evaluation of its acute oral toxicity study, *in vivo* antithrombotic efficacy, and associated bleeding risk assessment in rats.

Acute Oral Toxicity Study. Prior to the *in vivo* pharmacodynamics evaluation, the acute oral toxicity study of compound **24w** was carried out to investigate its preliminary toxicity profile in healthy mice according to Organization for Economic Cooperation and Development (OECD) guidelines.[71] The mice were carefully observed for any behavioral change and mortality after the oral administration of compound **24w** at a single dose of 2000 mg/kg. No death occurred after oral administration, and all mice in the drug administration group (male and female) grew normally compared to the mice in the control group. The body weights of these mice gradually increased during the subsequent 14 days (Figure 9), and no significant behavioral abnormalities were observed.

In Vivo* Antithrombotic Efficacy.** On the basis of the better *in vitro* antiplatelet potency and excellent PK properties, *in vivo* antithrombotic efficacy of compound **24w** was further evaluated and ticagrelor was tested for comparison as a positive control. The thrombus weights in compound **24w** and ticagrelor groups were significantly reduced compared to that of the model group (P < 0.001 for 5, 10, and 20 mg/kg of **24w** and 10 mg/kg of ticagrelor vs model; Figure 10), indicating that this ferric chloride model in rats was successfully established,[11,72−74] and compound **24w** as well as ticagrelor both resulted in a remarkable antithrombotic effect. Among them, the oral administration of compound **24w** demonstrated dose-dependent antithrombotic efficacy, achieving thrombus weight reductions of 22.6%, 40.7%, and 46.7% at doses of 5, 10, and 20 mg/kg, respectively. These results showed that its antithrombotic ED_{50} was 20.8 mg/kg. Specifically, compound **24w** (10 mg/kg) resulted in a thrombus weight reduction of 40.7%, which was comparable to that of ticagrelor (39.2%) at the same 10 mg/kg dose ($^{\#}P$ > 0.05 for 10 mg/kg **24w** vs ticagrelor). Consequently, the results of *in vivo* antithrombotic efficacy evaluation suggested that compound **24w** could be a potentially efficacious antithrombotic agent in the treatment of thrombotic disorders.

Bleeding Risk Assessment. Since bleeding complications had largely been considered an expected complication of antiplatelet therapy for all currently approved oral $P2Y_{12}$ antagonists,[11,28,43] the bleeding effect of compound **24w** was further evaluated in a rat-tail-bleeding model.[11,44,72] In this study, the bleeding effect of compound **24w** was compared to those of ticagrelor by measuring the tail-vein-bleeding time and

https://dx.doi.org/10.1021/acs.jmedchem.0c01524
J. Med. Chem. XXXX, XXX, XXX−XXX

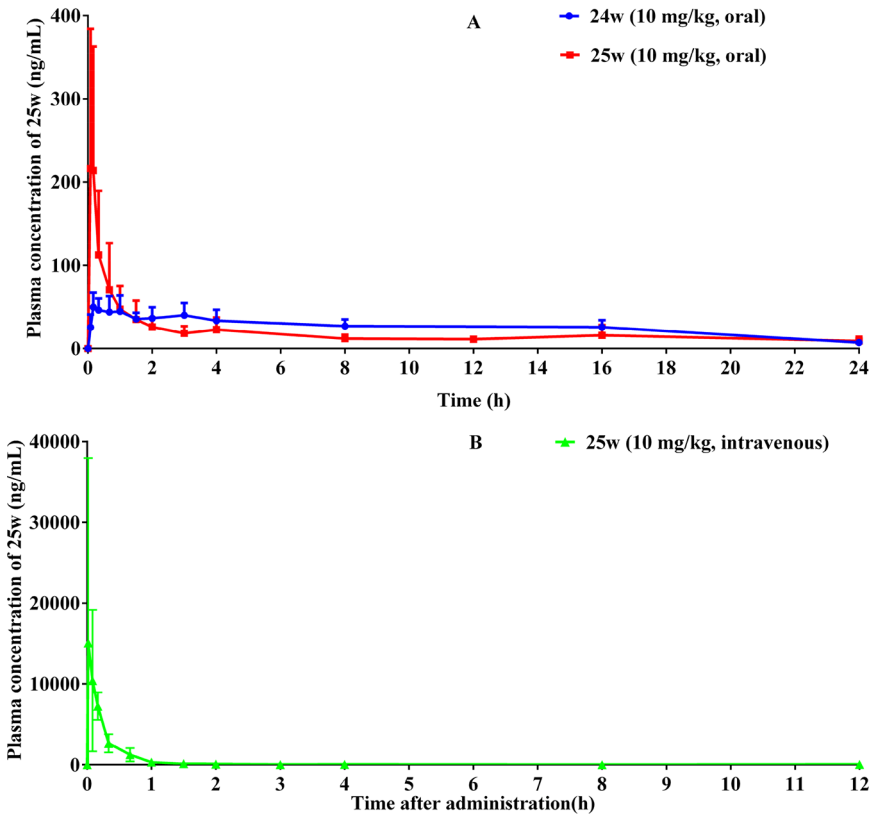

Figure 8. Plasma concentration−time profiles of compounds **24w** and **25w** after administration in rats (n = 6). (A) Single oral administration of compounds **24w** (parent compound **25w** released from prodrug **24w**; 10 mg/kg) and **25w** (10 mg/kg). (B) Intravenous injection administration of compound **25w** (10 mg/kg). Data are presented as the mean ± SD.

Table 6. Main Pharmacokinetic Parameters of Compounds 24w and 25w in Sprague-Dawley Rats after Administration (n = 6)[a]

parameters	oral administration (mean ± SD; **24w**)	oral administration (mean ± SD; **25w**)	intravenous administration (mean ± SD; **25w**)
C_{max} (ng/mL)	67.99 ± 10.72	214.05 ± 148.88	11225.0 ± 8214.12
T_{max} (h)	0.46 ± 0.29	0.167	0.14 ± 0.04
$AUC_{0-\infty}$ (ng·h/mL)	1135.08 ± 764.28	808.86 ± 382.05	3500.34 ± 1003.87
$t_{1/2}$ (h)	13.83 ± 10.82	13.13 ± 15.06	4.89 ± 3.24
CLz ($L \cdot h^{-1} \cdot kg^{-1}$)	12.40 ± 6.38	15.64 ± 8.64	3.03 ± 0.73
Vz (L/kg)	190.56 ± 86.64	239.60 ± 183.57	21.29 ± 15.29

[a] C_{max}, peak plasma concentration; T_{max}, time to reach C_{max}; $AUC_{0-\infty}$, area under the concentration−time curve from time zero to infinity; $t_{1/2}$, elimination half-life; CLz, clearance; Vz, volume of distribution.

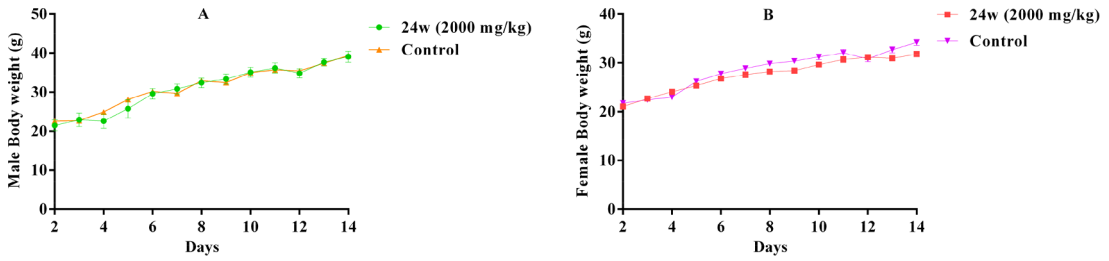

Figure 9. Body weight evolution of (A) male and (B) female mice. Each value is the mean ± SEM; n = 8.

weights in rats after oral administration. As shown in Figure 11, the blood loss of the vehicle-treated rats within 2 h after the tail snip amounted to 0.08 g with a bleeding time of 17.69 min, indicating that this assay was highly reproducible.[44,72] In ticagrelor-treated rats, the total bleeding time and weight were significantly increased by 6.78-fold and 48.63-fold in comparison to the vehicle, respectively (120 vs 17.69 min, 3.89 vs 0.08 g, ***P < 0.001 for ticagrelor group vs vehicle group). Compound **24w** only caused 1.92- and 5.00-times more than those of the vehicle group in bleeding time and

https://dx.doi.org/10.1021/acs.jmedchem.0c01524
J. Med. Chem. XXXX, XXX, XXX−XXX

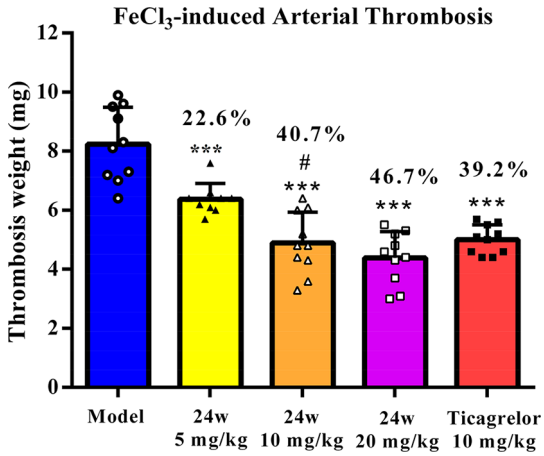

Figure 10. Effects of ticagrelor and compound **24w** on thrombus weight after $FeCl_3$-induced arterial injury in anesthetized Sprague-Dawley rats at 1.5 h postdosing following the oral administration of **24w** (5, 10, and 20 mg/kg) and ticagrelor (10 mg/kg). Data are presented as the mean ± SD (n = 10, ***P < 0.001 and ***P < 0.001 vs model; $^{\#}P$ > 0.05 vs ticagrelor).

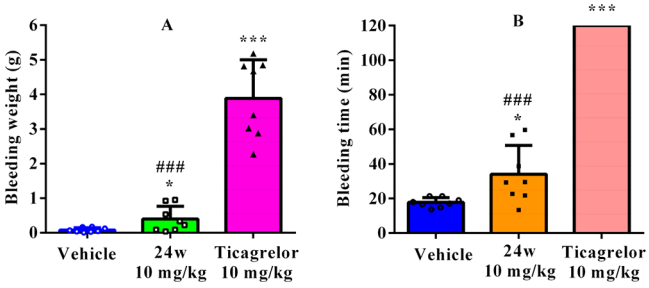

Figure 11. Effects of ticagrelor and compound **24w** on (A) tail-vein-bleeding weight and (B) time in anesthetized Sprague-Dawley rats at 2 h postdosing following the oral administration of **24w** (10 mg/kg) and ticagrelor (10 mg/kg). The data are presented as mean ± SD (n = 8, *P < 0.05, ***P < 0.001 vs model group; $^{\#\#\#}P$ < 0.001 vs ticagrelor group).

weight, respectively (33.94 vs 17.69 min, 0.40 vs 0.08 g, *P < 0.05 for **24w** group vs vehicle group), and were 3.54- and 9.73-times less than those of ticagrelor on the bleeding time and weight, respectively (33.94 vs 120 min, 0.40 vs 3.89 g, $^{\#\#\#}P$ < 0.001 for **24w** group vs ticagrelor group). These results indicated that **24w** resulted in much less blood loss than ticagrelor in rats at a therapeutically equivalent antithrombotic dose of 10 mg/kg. It was observed that, at this oral dose, compound **24w** could lead to a thrombosis inhibition of 40.7%, which was comparable to that of ticagrelor (39% inhibition of thrombosis). This reduction in bleeding time and weight when compared to ticagrelor indicated that compound **24w** clearly had a wider therapeutic window than ticagrelor in a rat thrombosis model and could potentially resolve the serious concern of high bleeding risk associated with clinical oral $P2Y_{12}$ antagonists.[14,16,35,36]

CONCLUSIONS

Starting from our previously reported nonpurine XO inhibitor **WSJ-557** with an apparent antiplatelet aggregation potency (IC_{50} = 15.727 μM), the 2-phenyl-1*H*-imidazole moiety was adopted as a new chemical scaffold for the structural optimization to lead to the identification of the most potent antiplatelet agents **24w** and **25w** (IC_{50} = 4.237 and 3.875 μM, respectively). We completed the optimization process and SAR of the target compounds. Moreover, $P2Y_1$-mediated cytosolic Ca^{2+} increase indicated that compound **25w** exhibited a potent inhibitory effect for $P2Y_1$ with a IC_{50} value of 2.59 μM, comparable with that of BPTU (IC_{50} = 3.03 μM), and $P2Y_{12}$-mediated vasodilator-stimulated phosphoprotein phosphorylation assay revealed that compound **25w** also could dose dependently antagonize $P2Y_{12}$ receptor, which could confirm that compound **25w** exerted its antiplatelet effect through both $P2Y_1$ and $P2Y_{12}$. Molecular modeling studies revealed the binding modes of **24w** and **25w** with two receptors, $P2Y_1$ and $P2Y_{12}$, which suggested that they could form hydrogen-bond interactions with key residues in active pockets. The simulated gastric and intestinal fluid stabilities indicated that they were considerably stable within 10 h, and the *in vitro* plasma and liver microsomal stability studies also showed that compound **24w** could be rapidly converted to compound **25w**. In addition, the CYP450 inhibition assay suggested that compound **25w** showed no apparent drug−drug interaction at 10 μM and there might be low liability for drug−drug interactions between **24w** and CYP2D6. Furthermore, the PK studies showed the T_{max} values of compounds **24w** and **25w** were 0.46 and 0.167 h, respectively, suggesting that they were both absorbed quickly into circulation, which could hopefully overcome the slow onset of action of currently approved oral $P2Y_{12}$ antagonists. The acute oral toxicity study of compound **24w** was evaluated in mice, and the results indicated that **24w** was nontoxic and tolerated at a dose up to 2000 mg/kg in mice. In addition, the rat ferric chloride model study suggested that compound **24w** demonstrated the dose-dependent antithrombotic efficacy and was comparable to what was observed for ticagrelor at the same oral dose (10 mg/kg). Importantly, compound **24w** showed significantly lower bleeding weight and time compared to ticagrelor at therapeutically equivalent antithrombotic dose (10 mg/kg) in a rat-tail-bleeding model, indicating that it had a clearly wider therapeutic window than ticagrelor in rats. This could potentially address the concern of high bleeding risk in clinically approved oral $P2Y_{12}$ antagonists. Therefore, compounds **24w** and **25w** were promising drug candidates for the treatment of arterial thrombosis and related diseases. The investigations performed in this research perfectly achieved the transition from a nonpurine imidazole XO inhibitor to dual-target $P2Y_1$ and $P2Y_{12}$ antagonists, which implied that other nonpurine XO inhibitors with a similar chemical structure to **WSJ-557** could also be adopted to design novel effective dual-target $P2Y_1$ and $P2Y_{12}$ antagonists.

EXPERIMENTAL SECTION

Chemistry. Compounds **WSJ-557** and **18** were prepared from our previous report,[51,52] and the purity of each was more than 95%. In addition, reagents and solvents were purchased from commercial sources and used without further purification. All reactions were monitored by TLC using silica gel aluminum cards (0.2 mm thickness) with 254 and 365 nm fluorescent indicators. Melting points were obtained using a YRT-3 melting apparatus and were uncorrected. ^{1}H NMR spectra were recorded on a Bruker 400 or 600 MHz spectrometer, and ^{13}C NMR spectra were recorded on a Bruker 400 or 600 MHz spectrometer. Chemical shifts were expressed in parts per million using tetramethylsilane as an internal reference and DMSO-d_6 as the solvent. Electrospray ionization-mass spectrometry (ESI-MS) data were gathered using an Agilent 1100 instrument and ESI-HRMS data were recorded in an Agilent 6540 Series quadrupole

https://dx.doi.org/10.1021/acs.jmedchem.0c01524
J. Med. Chem. XXXX, XXX, XXX−XXX

time-of-flight mass spectrometer (Q-TOF-MS) system (Supporting Information).

Ethyl 2-Hydroxyimino-3-oxobutanoate (20). A solution of sodium nitrite (51.3 g, 0.74 mol) in water (102.6 mL) was added dropwise at 0−5 °C to a stirred solution of ethyl acetoacetate (80 g, 0.62 mol) in acetic acid (240 mL). Upon completion of the reaction, a mixture of DCM (500 mL) and water (250 mL) was added. The organic phase was washed with water (2 × 150 mL) and brine (150 mL), dried (Na_2SO_4), and concentrated to afford a crude product **20** as a yellow oil, which was used for the next reaction without further purification.

Ethyl 2-(3-Cyanophenyl)-1-hydroxy-4-methyl-1*H*-imidazole-5-carboxylate (21a). A mixture of 3-formylbenzonitrile (30g, 0.229 mol), ethyl 2-hydroxyimino-3-oxobutanoate (43.7 g, 0.285 mol), ammonium acetate (176.3 g, 2.29 mol), and acetic acid (600 mL) was stirred at 50 °C under a nitrogen atmosphere for 24 h. The reaction mixture was cooled to room temperature and then slowly poured into cold water (2000 mL). The resulting precipitate was filtered, dried, and washed with ethyl acetate to obtain the compound **21a** as a white solid, yield: 75.5%. Purity (HPLC): 98.4%. Mp 167.7−170.2 °C. ESI-HRMS calcd. for $C_{14}H_{13}N_3O_3$ $[M + H]^+$ 272.1030, found: 272.1057. ^{1}H NMR (400 MHz, DMSO-d_6): δ 12.28 (s, 1H), 8.39 (t, J = 1.7 Hz, 1H), 8.34 (dt, J = 8.1, 1.4 Hz, 1H), 7.91 (dt, J = 7.8, 1.4 Hz, 1H), 7.71 (t, J = 7.9 Hz, 1H), 4.30 (q, J = 7.1 Hz, 2H), 2.39 (s, 3H), 1.32 (t, J = 7.1 Hz, 3H). ^{13}C NMR (100 MHz, DMSO-d_6): δ 159.33, 142.72, 141.14, 133.16, 132.35, 131.03, 130.49, 129.77, 118.94, 118.83, 112.29, 60.53, 16.14, 14.67.

Ethyl 2-(2-Cyanophenyl)-1-hydroxy-4-methyl-1*H*-imidazole-5-carboxylate (21b). Compound **21b** was prepared in the same manner as that described for **21a** and yielded a brown oil, which was used for the next reaction without further purification.

Ethyl 2-(4-Cyanophenyl)-1-hydroxy-4-methyl-1*H*-imidazole-5-carboxylate (21c). Compound **21c** was prepared in the same manner as that described for **21a** to yield a white solid, yield: 72.8%. Mp 170.5−171.8 °C. ^{1}H NMR (400 MHz, DMSO-d_6): δ 12.36 (s, 1H), 8.22 (d, J = 8.4 Hz, 2H), 7.93 (d, J = 8.4 Hz, 2H), 4.29 (q, J = 7.1 Hz, 2H), 2.38 (s, 3H), 1.31 (t, J = 7.1 Hz, 3H).

Ethyl 1-Hydroxy-4-methyl-2-phenyl-1*H*-imidazole-5-carboxylate (21d). Compound **21d** was prepared in the same manner as that described for **21a** to yield a white solid, yield: 83.7%. Mp 131.5−133.1 °C. ESI-MS m/z: 247.1 $[M + H]^+$. ^{1}H NMR (400 MHz, DMSO-d_6): δ 8.22−8.13 (m, 2H), 7.46−7.33 (m, 3H), 4.23 (q, J = 7.1 Hz, 2H), 2.34 (s, 3H), 1.28 (t, J = 7.1 Hz, 3H).

Ethyl 2-(3-Cyanophenyl)-1-methoxy-4-methyl-1*H*-imidazole-5-carboxylate (22a). A solution of compound **21a** (0.51 g, 2.0 mmol), anhydrous potassium carbonate (0.33g, 2.40 mmol), and iodomethane (0.33 g, 2.4 mmol) in DMF (5.4 mL) was stirred at 35 °C under a nitrogen atmosphere for 1 h. After the completion of the reaction, the reaction mixture was poured into 11 mL of water and stirred for 10 min. The precipitate was filtered and washed with water, and then, ethyl acetate (5.0 mL) was added to wash residue to yield compound **22a** as a white solid, yield: 79.3%. Purity (HPLC): 99.5%. Mp 122.4−123.5 °C. ESI-HRMS calcd. for $C_{15}H_{15}N_3O_3$ $[M + H]^+$ 285.1186, found: 286.1207. ^{1}H NMR (400 MHz, DMSO-d_6): δ 8.37−8.27 (m, 2H), 7.97 (dt, J = 7.6, 1.4 Hz, 1H), 7.75 (t, J = 7.8 Hz, 1H), 4.32 (q, J = 7.1 Hz, 2H), 3.98 (s, 3H), 2.40 (s, 3H), 1.33 (t, J = 7.1 Hz, 3H). ^{13}C NMR (100 MHz, DMSO-d_6): δ 158.68, 143.82, 140.26, 133.78, 132.14, 130.90, 130.82, 129.02, 118.70, 116.97, 112.70, 67.65, 60.84, 16.23, 14.54.

Ethyl 2-(2-Cyanophenyl)-1-methoxy-4-methyl-1*H*-imidazole-5-carboxylate (22b). Compound **22b** was prepared in the same manner as that described for **22a** to yield a yellow solid, yield: 51.4%. Purity (HPLC): 99.3%. Mp 144.2−145.6 °C. ESI-MS m/z: 286.17 $[M + H]^+$. ^{1}H NMR (400 MHz, DMSO-d_6): δ 7.68−7.57 (m, 3H), 7.52 (dd, J = 7.4, 1.4 Hz, 1H), 4.32 (q, J = 7.1 Hz, 2H), 3.79 (s, 3H), 2.42 (s, 3H), 1.33 (t, J = 7.1 Hz, 3H). ^{13}C NMR (100 MHz, DMSO-d_6): δ 158.69, 143.83, 140.26, 133.76, 132.12, 130.90, 130.81, 129.04, 118.69, 116.98, 112.71, 67.64, 60.83, 16.21, 14.53.

Ethyl 2-(4-Cyanophenyl)-1-methoxy-4-methyl-1*H*-imidazole-5-carboxylate (22c). Compound **22c** was prepared in the same manner as that described for **22a** to yield a white solid, yield: 92.4%. Purity (HPLC): 98.1%. Mp 147.3−148.5 °C. ESI-HRMS calcd. for $C_{15}H_{15}N_3O_3$ $[M + H]^+$ 286.1186, found: 286.1208. ^{1}H NMR (400 MHz, DMSO-d_6): δ 8.21 (dd, 2H), 7.99 (dd, 2H), 4.33 (q, J = 7.1 Hz, 2H), 3.98 (s, 3H), 2.42 (s, 3H), 1.34 (t, J = 7.1 Hz, 3H). ^{13}C NMR (100 MHz, DMSO-d_6): δ 158.67, 143.97, 140.37, 133.37, 131.94, 128.22, 118.88, 117.29, 112.53, 67.72, 60.90, 16.28, 14.55.

Ethyl 1-Methoxy-4-methyl-2-phenyl-1*H*-imidazole-5-carboxylate (22d). Compound **22d** was prepared in the same manner as that described for **22a** to yield a white solid, yield: 88.5%. Purity (HPLC): 99.8%. Mp 98.8−100.4 °C. ESI-HRMS calcd. for $C_{14}H_{16}N_2O_3$ $[M + H]^+$ 261.1234, found: 261.1300. ^{1}H NMR (600 MHz, DMSO-d_6): δ 8.10−7.99 (m, 2H), 7.57−7.45 (m, 3H), 4.30 (q, J = 7.1 Hz, 2H), 3.93 (s, 3H), 2.40 (s, 3H), 1.32 (t, J = 7.1 Hz, 3H). ^{13}C NMR (100 MHz, DMSO-d_6): δ 158.84, 143.68, 142.27, 130.39, 129.36, 127.95, 127.72, 116.35, 67.21, 60.62, 16.28, 14.57.

Ethyl 2-(3-Cyanophenyl)-4-methyl-1*H*-imidazole-5-carboxylate (23). A suspension of compound **21a** (2.6 g, 10 mmol), potassium iodide (1.16g, 10 mmol), chlorotrimethylsilane (1.63g, 15 mmol), and acetonitrile (30 mL) was stirred at 60 °C for 6 h. The reaction mixture was poured into a solution of 1 M sodium hydroxide aqueous and was stirred for 1 h. The precipitate was filtered and washed with ethyl acetate to obtain compound **23** as a white solid, yield: 77.3%. Purity (HPLC): 97.7%. Mp 209.6−210.7 °C. ESI-HRMS calcd. for $C_{15}H_{15}N_3O_2$ $[M - H]^-$ 254.0935, found: 254.0959. ^{1}H NMR (400 MHz, DMSO-d_6): δ 8.35 (s, 1H), 8.28 (d, J = 8.0 Hz, 1H), 7.80 (d, J = 7.7 Hz, 1H), 7.65 (t, J = 7.8 Hz, 1H), 4.80 (s, 1H), 4.25 (q, J = 7.1 Hz, 2H), 2.47 (s, 3H), 1.30 (t, J = 7.1 Hz, 3H). ^{13}C NMR (100 MHz, DMSO-d_6): δ 162.99, 144.34, 140.85, 132.04, 130.50, 130.13, 128.92, 126.99, 118.97, 112.31, 59.83, 14.86, 12.89.

Ethyl 2-(3-Cyanophenyl)-1,4-dimethyl-1*H*-imidazole-5-carboxylate (24a). A solution of compound **23** (0.51 g, 2.0 mmol), anhydrous potassium carbonate (0.33g, 2.40 mmol), and iodomethane (0.33 g, 2.4 mmol) in DMF (5.4 mL) was stirred at 35 °C under a nitrogen atmosphere for 1 h. After the completion of the reaction, the reaction mixture was poured into 11 mL of water and stirred for 10 min. The precipitate was filtered and washed with water, and then, ethyl acetate (5.0 mL) was added to wash the residue to yield compound **24a** as a white solid, yield: 76.2%. Purity (HPLC): 97.9%. Mp 137.3−138.1 °C. ESI-HRMS calcd. for $C_{15}H_{15}N_3O_2$ $[M + H]^+$ 270.1237, found: 270.1250. ^{1}H NMR (400 MHz, DMSO-d_6): δ 8.13 (s, 1H), 8.07−7.91 (m, 2H), 7.73 (t, J = 7.8 Hz, 1H), 4.30 (q, J = 7.3 Hz, 2H), 3.84 (s, 3H), 2.42 (s, 3H), 1.33 (t, J = 7.1 Hz, 3H). ^{13}C NMR (100 MHz, DMSO-d_6): δ 160.95, 148.48, 146.87, 134.35, 133.45, 132.92, 131.23, 130.38, 120.94, 118.74, 112.32, 60.54, 35.03, 16.05, 14.65.

Ethyl 2-(3-Cyanophenyl)-1-isopropyl-4-methyl-1*H*-imidazole-5-carboxylate (24b). Compound **23** (0.51 g, 2.0 mmol), anhydrous potassium carbonate (0.33 g, 2.4 mmol), potassium iodide (39.84 mg, 0.24 mmol), and 2-bromopropane (295 mg, 2.4 mmol) were dissolved in DMF (5.4 mL), and the reaction mixture was stirred at 35 °C for 1 h. Then, the mixture was poured into water (11 mL) and stirred for 10 min, which was filtered and washed with ethyl acetate to provide the compound **24b** as a white solid, yield: 68.3%. Purity (HPLC): 99.2%. Mp 105.3−106.7 °C. ESI-MS m/z: 298.2 $[M + H]^+$. ^{1}H NMR (400 MHz, DMSO-d_6): δ 8.33−8.24 (m, 2H), 7.94 (d, J = 7.7 Hz, 1H), 7.73 (t, J = 7.8 Hz, 1H), 4.44 (hept, J = 6.2 Hz, 1H), 4.30 (q, J = 7.1 Hz, 2H), 2.41 (s, 3H), 1.32 (t, J = 7.1 Hz, 3H), 1.03 (d, J = 6.0 Hz, 6H). ^{13}C NMR (100 MHz, DMSO-d_6): δ 158.90, 144.08, 142.05, 133.54, 132.72, 131.59, 130.54, 129.89, 118.62, 117.68, 112.39, 83.52, 60.76, 20.24, 16.32, 14.55.

Ethyl 2-(3-Cyanophenyl)-1-isopropoxy-4-methyl-1*H*-imidazole-5-carboxylate (24c). A mixture of compound **21a** (0.54 g, 2.0 mmol), 2-bromopropane (295 mg, 2.4 mmol), anhydrous potassium carbonate (0.33 g, 2.4 mmol), potassium iodide (39.84 mg, 0.24 mmol), and DMF (5.4 mL) was reacted at 35 °C for 1 h under a nitrogen atmosphere. After the reaction was completed, the mixture was poured into water (11.0 mL) and stirred for 10 min. The precipitate was filtered, washed with water, and stirred for 30 min in a

https://dx.doi.org/10.1021/acs.jmedchem.0c01524
J. Med. Chem. XXXX, XXX, XXX−XXX

solution of ethyl acetate (5.0 mL), which was filtered to yield compound **24c** as a white solid, yield: 79.3%. Purity (HPLC): 99.4%. Mp 99.6−101.5 °C. ESI-HRMS calcd. for $C_{17}H_{19}N_3O_3$ $[M + H]^+$ 314.1499, found: 314.1513. ^{1}H NMR (600 MHz, DMSO-d_6): δ 8.31 (t, J = 1.7 Hz, 1H), 8.29 (dt, J = 8.0, 1.4 Hz, 1H), 7.95 (dt, J = 7.8, 1.4 Hz, 1H), 7.74 (t, J = 7.9 Hz, 1H), 4.44 (h, J = 6.2 Hz, 1H), 4.31 (q, J = 7.1 Hz, 2H), 2.42 (s, 3H), 1.33 (t, J = 7.1 Hz, 3H), 1.14−0.93 (m, 6H). ^{13}C NMR (100 MHz, DMSO-d_6): δ 158.93, 144.09, 142.11, 133.62, 132.78, 131.64, 130.60, 129.87, 118.66, 117.67, 112.39, 83.57, 60.81, 20.27, 16.36, 14.59.

Ethyl 1-(Allyloxy)-2-(3-cyanophenyl)-4-methyl-1*H*-imidazole-5-carboxylate (24d). Compound **24d** was prepared in the same manner as that described for **24c** to yield a white solid, yield: 73.1%. Purity (HPLC): 99.6%. Mp 94.7−96.2 °C. ESI-HRMS calcd. for $C_{17}H_{17}N_3O_3$ $[M + H]^+$ 312.1343, found: 312.1361. ^{1}H NMR (600 MHz, DMSO-d_6): δ 8.34−8.32 (m, 1H), 8.31−8.27 (m, 1H), 7.97 (dt, J = 7.8, 1.4 Hz, 1H), 7.79−7.72 (m, 1H), 5.95−5.76 (m, 1H), 5.41−5.25 (m, 2H), 4.66 (d, J = 6.4 Hz, 2H), 4.32 (q, J = 7.1 Hz, 2H), 2.41 (s, 3H), 1.33 (t, J = 7.1 Hz, 3H). ^{13}C NMR (100 MHz, DMSO-d_6): δ 158.83, 143.83, 140.95, 133.69, 132.35, 131.11, 130.71, 129.33, 123.02, 118.66, 112.56, 80.69, 60.85, 16.24, 14.56.

Ethyl 2-(3-Cyanophenyl)-1-(2-ethoxyethoxy)-4-methyl-1*H*-imidazole-5-carboxylate (24e). Compound **24e** was prepared in the same manner as that described for **24c** to yield a white solid, yield: 83.2%. Purity (HPLC): 97.5%. Mp 88.6−89.4 °C. ESI-HRMS calcd. for $C_{18}H_{21}N_3O_4$ $[M + H]^+$ 344.1605, found: 344.1619. ^{1}H NMR (600 MHz, DMSO-d_6): δ 8.46 (t, J = 1.7 Hz, 1H), 8.39 (dt, J = 8.1, 1.4 Hz, 1H), 7.95 (dt, J = 7.7, 1.3 Hz, 1H), 7.70 (t, J = 7.9 Hz, 1H), 4.37−4.25 (m, 4H), 3.59 (dd, J = 4.9, 3.2 Hz, 2H), 3.35−3.33 (m, 2H), 2.40 (s, 3H), 1.32 (t, J = 7.1 Hz, 3H), 1.09 (t, J = 7.0 Hz, 3H). ^{13}C NMR (100 MHz, DMSO-d_6): δ 158.76, 143.93, 133.67, 132.57, 131.07, 130.45, 128.97, 118.76, 117.18, 112.48, 79.70, 67.18, 66.16, 60.84, 16.25, 15.30, 14.52.

Ethyl 2-(3-Cyanophenyl)-1-(2-ethoxy-2-oxoethoxy)-4-methyl-1*H*-imidazole-5-carboxylate (24f). Compound **24f** was prepared in the same manner as that described for **24c** to yield a white solid, yield: 79.8%. Purity (HPLC): 99.0%. Mp 126.3−127.7 °C. ESI-HRMS calcd. for $C_{18}H_{19}N_3O_5$ $[M + H]^+$ 358.1397, found: 358.1431. ^{1}H NMR (600 MHz, DMSO-d_6): δ 8.41 (s, 1H), 8.33 (dt, J = 8.1, 1.4 Hz, 1H), 7.96 (dt, J = 7.8, 1.4 Hz, 1H), 7.73 (t, J = 7.9 Hz, 1H), 4.95 (s, 2H), 4.31 (q, J = 7.1 Hz, 2H), 4.13 (q, J = 7.1 Hz, 2H), 2.41 (s, 3H), 1.31 (t, J = 7.1 Hz, 3H), 1.18 (t, J = 7.1 Hz, 3H). ^{13}C NMR (100 MHz, DMSO-d_6): δ 166.39, 158.74, 143.85, 140.75, 133.76, 132.54, 131.19, 130.58, 129.05, 118.72, 117.20, 112.51, 75.54, 61.60, 61.00, 16.26, 14.44, 14.32.

Ethyl 2-(3-Cyanophenyl)-1-(3-hydroxypropoxy)-4-methyl-1*H*-imidazole-5-carboxylate (24g). Compound **24g** was prepared in the same manner as that described for **24c** to yield a white solid, yield: 66.4%. Purity (HPLC): 95.8%. Mp 78.6−80.4 °C. ESI-HRMS calcd. for $C_{17}H_{19}N_3O_4$ $[M + H]^+$ 330.1448, found: 330.1483. ^{1}H NMR (600 MHz, DMSO-d_6): δ 8.33 (t, J = 1.7 Hz, 1H), 8.30 (dt, J = 8.1, 1.4 Hz, 1H), 7.96 (dt, J = 7.7, 1.4 Hz, 1H), 7.74 (t, J = 7.9 Hz, 1H), 4.54 (t, J = 5.1 Hz, 1H), 4.31 (q, J = 7.1 Hz, 2H), 4.15 (t, J = 6.5 Hz, 2H), 3.48 (q, J = 6.0 Hz, 2H), 2.40 (s, 3H), 1.80 (p, J = 6.5 Hz, 2H), 1.33 (t, J = 7.1 Hz, 3H). ^{13}C NMR (100 MHz, DMSO-d_6): δ 158.78, 143.93, 140.66, 133.71, 132.24, 131.09, 130.72, 129.10, 118.64, 117.08, 112.62, 78.14, 60.83, 57.62, 31.26, 16.22, 14.57.

Ethyl 1-(2-Amino-2-oxoethoxy)-2-(3-cyanophenyl)-4-methyl-1*H*-imidazole-5-carboxylate (24h). Compound **24h** was prepared in the same manner as that described for **24c** to yield a white solid, yield: 86.7%. Purity (HPLC): 96.7%. Mp 179.6−181.2 °C. ESI-HRMS calcd. for $C_{16}H_{16}N_4O_4$ $[M + H]^+$ 329.1244, found: 329.1364. ^{1}H NMR (600 MHz, DMSO-d_6): δ 8.51 (t, J = 1.7 Hz, 1H), 8.38 (dt, J = 8.1, 1.5 Hz, 1H), 7.95 (dt, J = 7.8, 1.4 Hz, 1H), 7.72 (t, J = 7.9 Hz, 1H), 7.66 (s, 1H), 7.54 (s, 1H), 4.62 (s, 2H), 4.31 (q, J = 7.1 Hz, 2H), 2.41 (s, 3H), 1.32 (t, J = 7.1 Hz, 3H). ^{13}C NMR (100 MHz, DMSO-d_6): δ 167.20, 158.79, 143.89, 140.67, 133.84, 132.48, 131.19, 130.59, 128.94, 118.71, 117.15, 112.63, 77.05, 61.00, 16.23, 14.47.

3-{[2-(3-Cyanophenyl)-5-(ethoxycarbonyl)-4-methyl-1*H*-imidazol-1-yl] oxy} Propanoic acid (24i). Compound **24i** was prepared in the same manner as that described for **24c** to yield a white solid, yield: 75.4%. Purity (HPLC): 99.0%. Mp 142.1−143.9 °C. ESI-MS m/z: 344.2 $[M + H]^+$. ^{1}H NMR (400 MHz, DMSO-d_6): δ 12.52 (s, 1H), 8.43−8.30 (m, 2H), 7.95 (d, J = 7.7 Hz, 1H), 7.71 (t, J = 7.9 Hz, 1H), 4.47−4.18 (m, 4H), 2.67 (t, J = 5.9 Hz, 2H), 2.41 (s, 3H), 1.33 (t, J = 7.1 Hz, 3H). ^{13}C NMR (100 MHz, DMSO-d_6): δ 171.77, 158.80, 143.95, 140.78, 133.80, 132.41, 131.23, 130.59, 128.94, 118.67, 117.07, 112.68, 76.00, 60.87, 33.14, 16.26, 14.58.

Ethyl 2-(3-Cyanophenyl)-4-methyl-1-(pyridin-4-ylmethoxy)-1*H*-imidazole-5-carboxylate (24j). Compound **24j** was prepared in the same manner as that described for **24c** to yield a white solid, yield: 76.2%. Purity (HPLC): 99.2%. Mp 133.5−135.1 °C. ESI-HRMS calcd. for $C_{20}H_{18}N_4O_3$ $[M + H]^+$ 363.1452, found: 363.1471. ^{1}H NMR (600 MHz, DMSO-d_6): δ 8.58−8.42 (m, 2H), 8.14 (t, J = 1.7 Hz, 1H), 8.11 (dt, J = 8.1, 1.4 Hz, 1H), 7.92 (dt, J = 7.8, 1.4 Hz, 1H), 7.66 (t, J = 7.9 Hz, 1H), 7.31−7.23 (m, 2H), 5.19 (s, 2H), 4.34 (q, J = 7.1 Hz, 2H), 2.44 (s, 3H), 1.31 (t, J = 7.1 Hz, 3H). ^{13}C NMR (150 MHz, DMSO-d_6): δ 158.87, 150.26, 144.02, 141.67, 133.67, 132.49, 131.32, 130.55, 128.99, 124.24, 118.59, 116.95, 112.37, 79.87, 60.97, 16.36, 14.57.

Ethyl 1-(Benzyloxy)-2-(3-cyanophenyl)-4-methyl-1*H*-imidazole-5-carboxylate (24k). Compound **24k** was prepared in the same manner as that described for **24c** to yield a white solid, yield: 94.3%. Purity (HPLC): 98.5%. Mp 124.8−126.3 °C. ESI-HRMS calcd. for $C_{21}H_{20}N_3O_3$ $[M + H]^+$ 362.1499, found: 362.1539. ^{1}H NMR (600 MHz, DMSO-d_6): δ 8.13−8.09 (m, 2H), 7.90 (dt, J = 7.7, 1.4 Hz, 1H), 7.65 (td, J = 7.8, 0.6 Hz, 1H), 7.36−7.31 (m, 1H), 7.30−7.25 (m, 2H), 7.23−7.18 (m, 2H), 5.12 (s, 2H), 4.36 (q, J = 7.1 Hz, 2H), 2.43 (s, 3H), 1.35 (t, J = 7.1 Hz, 3H). ^{13}C NMR (100 MHz, DMSO-d_6): δ 158.93, 143.95, 141.46, 133.43, 132.95, 132.51, 131.21, 130.57, 130.35, 129.86, 129.17, 128.85, 118.62, 117.06, 112.25, 81.89, 60.90, 16.36, 14.63.

Ethyl 2-(3-Cyanophenyl)-1-[(2-fluorobenzyl)oxy]-4-methyl-1*H*-imidazole-5-carboxylate (24l). Compound **24l** was prepared in the same manner as that described for **24c** to yield a white solid, yield: 83.2%. Purity (HPLC): 95.9%. Mp 135.5−136.4 °C. ESI-HRMS calcd. for $C_{21}H_{18}FN_3O_3$ $[M + H]^+$ 380.1405, found: 380.1453. ^{1}H NMR (600 MHz, DMSO-d_6): δ 8.02 (s, 1H), 7.98 (d, J = 8.0 Hz, 1H), 7.86 (d, J = 7.7 Hz, 1H), 7.59 (t, J = 7.8 Hz, 1H), 7.32 (d, J = 6.9 Hz, 1H), 7.15 (t, J = 7.1 Hz, 1H), 7.05 (t, J = 7.4 Hz, 1H), 6.96 (t, J = 9.2 Hz, 1H), 5.20 (s, 2H), 4.35 (q, J = 7.0 Hz, 2H), 2.43 (s, 3H), 1.35 (t, J = 7.0 Hz, 3H). ^{13}C NMR (100 MHz, DMSO-d_6): δ 158.92, 144.05, 141.86, 133.33, 132.73, 132.65, 132.58, 131.25, 130.16, 129.03, 124.81, 124.78, 118.61, 116.96, 115.69, 115.48, 112.10, 75.22, 60.90, 16.34, 14.59.

Ethyl 2-(3-Cyanophenyl)-1-[(3-fluorobenzyl)oxy]-4-methyl-1*H*-imidazole-5-carboxylate (24m). Compound **24m** was prepared in the same manner as that described for **24c** to yield a white solid, yield: 76.9%. Purity (HPLC): 99.7%. Mp 136.3−138.0 °C. ESI-HRMS calcd. for $C_{21}H_{20}FN_3O_3$ $[M + H]^+$ 380.1405, found: 380.1464. ^{1}H NMR (600 MHz, DMSO-d_6): δ 8.12−8.03 (m, 2H), 7.90 (dt, J = 7.7, 1.4 Hz, 1H), 7.64 (t, J = 7.8 Hz, 1H), 7.36−7.26 (m, 1H), 7.19−7.12 (m, 1H), 7.10−6.98 (m, 2H), 5.15 (s, 2H), 4.35 (q, J = 7.1 Hz, 2H), 2.43 (s, 3H), 1.34 (t, J = 7.1 Hz, 3H). ^{13}C NMR (100 MHz, DMSO-d_6): δ 158.93, 144.04, 141.75, 135.30, 133.50, 133.48, 132.60, 131.30, 130.67, 130.52, 130.28, 129.75, 129.08, 129.06, 118.59, 116.94, 112.22, 80.84, 60.93, 16.36, 14.60.

Ethyl 2-(3-Cyanophenyl)-1-[(4-fluorobenzyl)oxy]-4-methyl-1*H*-imidazole-5-carboxylate (24n). Compound **24n** was prepared in the same manner as that described for **24c** to yield a white solid, yield: 82.7%. Purity (HPLC): 98.0%. Mp 140.7−141.8 °C. ESI-HRMS calcd. for $C_{21}H_{18}FN_3O_3$ $[M + H]^+$ 380.1405, found: 380.1472. ^{1}H NMR (600 MHz, DMSO-d_6): δ 8.12−8.02 (m, 2H), 7.89 (d, J = 7.7 Hz, 1H), 7.63 (t, J = 7.8 Hz, 1H), 7.22 (dd, J = 8.3, 5.5 Hz, 2H), 7.06 (t, J = 8.6 Hz, 2H), 5.11 (s, 2H), 4.35 (q, J = 7.1 Hz, 2H), 2.42 (s, 3H), 1.35 (t, J = 7.1 Hz, 3H). ^{13}C NMR (100 MHz, DMSO-d_6): δ 158.93, 143.99, 141.64, 133.40, 133.06, 132.97, 132.51, 131.25,

https://dx.doi.org/10.1021/acs.jmedchem.0c01524
J. Med. Chem. XXXX, XXX, XXX−XXX

130.28, 129.19, 118.60, 117.00, 115.80, 115.58, 112.18, 80.93, 60.90, 16.38, 14.62.

Ethyl 1-[(2-Chlorobenzyl)oxy]-2-(3-cyanophenyl)-4-methyl-1*H*-imidazole-5-carboxylate (24o). Compound **24o** was prepared in the same manner as that described for **24c** to yield a white solid, yield: 76.5%. Purity (HPLC): 98.4%. Mp 124.6−125.7 °C. ESI-HRMS calcd. for $C_{21}H_{18}ClN_3O_3$ $[M - H]^-$ 394.1037, found: 394.0975. ^{1}H NMR (400 MHz, DMSO-d_6): δ 7.96 (s, 1H), 7.90 (d, J = 8.0 Hz, 1H), 7.82 (d, J = 7.8 Hz, 1H), 7.54 (t, J = 7.9 Hz, 1H), 7.28−7.21 (m, 1H), 7.21−7.14 (m, 3H), 5.24 (s, 2H), 4.35 (q, J = 7.1 Hz, 2H), 2.43 (s, 3H), 1.35 (t, J = 7.1 Hz, 3H).^{13}C NMR (100 MHz, DMSO-d_6): δ 158.94, 144.16, 142.20, 134.86, 133.37, 133.22, 132.69, 131.89, 131.46, 130.81, 130.05, 129.62, 128.97, 127.55, 118.61, 116.86, 112.01, 78.84, 60.89, 16.38, 14.58.

Ethyl 1-[(3-Chlorobenzyl)oxy]-2-(3-cyanophenyl)-4-methyl-1*H*-imidazole-5-carboxylate (24p). Compound **24p** was prepared in the same manner as that described for **24c** to yield a white solid, yield: 83.8%. Purity (HPLC): 97.0%. Mp 118.3−119.7 °C. ESI-HRMS calcd. for $C_{21}H_{18}ClN_3O_3$ $[M + H]^+$ 396.1109, found: 396.1156. ^{1}H NMR (600 MHz, DMSO-d_6): δ 8.07−8.00 (m, 2H), 7.89 (dt, J = 7.8, 1.4 Hz, 1H), 7.63 (t, J = 7.8 Hz, 1H), 7.37−7.31 (m, 1H), 7.27 (t, J = 7.8 Hz, 1H), 7.24 (t, J = 1.8 Hz, 1H), 7.11 (dt, J = 7.5, 1.3 Hz, 1H), 5.14 (s, 2H), 4.35 (q, J = 7.1 Hz, 2H), 2.43 (s, 3H), 1.35 (t, J = 7.1 Hz, 3H). ^{13}C NMR (100 MHz, DMSO-d_6): δ 158.91, 144.03, 141.69, 135.29, 133.48, 132.57, 131.27, 130.66, 130.50, 130.27, 129.74, 129.05, 116.92, 112.22, 80.82, 60.92, 16.36, 14.59.

Ethyl 1-[(4-Chlorobenzyl)oxy]-2-(3-cyanophenyl)-4-methyl-1*H*-imidazole-5-carboxylate (24q). Compound **24q** was prepared in the same manner as that described for **24c** to yield a white solid, yield: 76.2%. Purity (HPLC): 99.6%. Mp 146.9−148.3 °C. ESI-HRMS calcd. for $C_{21}H_{18}ClN_3O_3$ $[M + H]^+$ 396.1109, found: 396.1170. ^{1}H NMR (400 MHz, DMSO-d_6): δ 8.07−8.02 (m, 2H), 7.89 (dt, J = 7.8, 1.4 Hz, 1H), 7.69−7.58 (m, 1H), 7.28 (d, J = 8.4 Hz, 2H), 7.18 (d, J = 8.4 Hz, 2H), 5.12 (s, 2H), 4.35 (q, J = 7.1 Hz, 2H), 2.43 (s, 3H), 1.35 (t, J = 7.1 Hz, 3H). ^{13}C NMR (100 MHz, DMSO-d_6): δ 158.91, 144.00, 134.82, 133.37, 132.49, 132.41, 131.93, 131.23, 130.24, 129.15, 128.81, 118.59, 112.18, 80.86, 60.90, 16.37, 14.61.

Ethyl 1-[(4-Bromobenzyl)oxy]-2-(3-cyanophenyl)-4-methyl-1*H*-imidazole-5-carboxylate (24r). Compound **24r** was prepared in the same manner as that described for **24c** to yield a white solid, yield: 79.4%. Purity (HPLC): 99.7%. Mp 137.6−139.3 °C. ESI-HRMS calcd. for $C_{21}H_{18}BrN_3O_3$ $[M + H]^+$ 440.0604, found: 440.0653. ^{1}H NMR (600 MHz, DMSO-d_6): δ 8.08−8.00 (m, 2H), 7.90 (d, J = 7.7 Hz, 1H), 7.63 (t, J = 7.7 Hz, 1H), 7.42 (d, J = 7.9 Hz, 2H), 7.11 (d, J = 7.9 Hz, 2H), 5.12 (s, 2H), 4.35 (q, J = 7.1 Hz, 2H), 2.43 (s, 3H), 1.35 (t, J = 7.1 Hz, 3H). ^{13}C NMR (100 MHz, DMSO-d_6): δ 158.88, 143.99, 141.57, 133.34, 132.63, 132.44, 132.28, 131.75, 131.20, 130.22, 129.12, 123.54, 118.58, 112.19, 80.91, 60.90, 16.37, 14.60.

Ethyl 2-(3-Cyanophenyl)-4-methyl-1-[(4-methylbenzyl)oxy]-1*H*-imidazole-5-carboxylate (24s). Compound **24s** was prepared in the same manner as that described for **24c** to yield a white solid, yield: 81.3%. Purity (HPLC): 99.2%. Mp 119.4−120.7 °C. ESI-HRMS calcd. for $C_{22}H_{21}N_3O_3$ $[M + H]^+$ 376.1656, found: 376.1745. ^{1}H NMR (600 MHz, DMSO-d_6): δ 8.07−8.01 (m, 2H), 7.89 (dt, J = 7.8, 1.3 Hz, 1H), 7.63 (t, J = 7.8 Hz, 1H), 7.05−6.98 (m, 4H), 5.06 (s, 2H), 4.36 (q, J = 7.1 Hz, 2H), 2.43 (s, 3H), 2.26 (s, 3H), 1.35 (t, J = 7.1 Hz, 3H). ^{13}C NMR (100 MHz, DMSO-d_6): δ 158.93, 143.97, 141.66, 139.54, 133.27, 132.56, 131.16, 130.64, 130.14, 129.88, 129.33, 129.21, 118.64, 116.97, 112.08, 81.75, 60.86, 21.24, 16.36, 14.62.

Ethyl 2-(3-Cyanophenyl)-1-[(4-methoxybenzyl)oxy]-4-methyl-1*H*-imidazole-5-carboxylate (24t). Compound **24t** was prepared in the same manner as that described for **24c** to yield a white solid, yield: 74.2%. Purity (HPLC): 99.3%. Mp 99.2−101.3 °C. ESI-HRMS calcd. for $C_{22}H_{21}N_3O_4$ $[M + H]^+$ 392.1605, found: 392.1635. ^{1}H NMR (400 MHz, DMSO-d_6): δ 8.09−8.00 (m, 2H), 7.87 (dt, J = 7.8, 1.5 Hz, 1H), 7.69−7.57 (m, 1H), 7.10−7.00 (m, 2H), 6.80−6.67 (m, 2H), 5.04 (s, 2H), 4.36 (q, J = 7.1 Hz, 2H), 3.72 (s, 3H), 2.42 (s, 3H), 1.36 (t, J = 7.1 Hz, 3H). ^{13}C NMR (100 MHz, DMSO-d_6): δ 160.64, 158.96, 143.99, 141.78, 133.26, 132.53, 132.35, 131.21, 130.15, 129.27, 124.83, 118.65, 116.96, 114.11, 112.07, 81.62, 60.85, 55.59, 16.39, 14.64.

Ethyl 2-(3-Cyanophenyl)-1-{[4-(methoxycarbonyl)benzyl]-oxy}-4-methyl-1*H*-imidazole-5-carboxylate (24u). Compound **24u** was prepared in the same manner as as that described for **24c** to yield a white solid, yield: 85.2%. Purity (HPLC): 97.4%. Mp 167.5−169.4 °C. ESI-HRMS calcd. for $C_{23}H_{21}N_3O_5$ $[M + H]^+$ 420.1554, found: 420.1676. ^{1}H NMR (400 MHz, DMSO-d_6): δ 8.05 (dt, J = 8.1, 1.4 Hz, 1H), 8.01 (t, J = 1.6 Hz, 1H), 7.88 (dt, J = 7.8, 1.3 Hz, 1H), 7.81 (d, J = 8.3 Hz, 2H), 7.62 (t, J = 7.9 Hz, 1H), 7.33 (d, J = 8.2 Hz, 2H), 5.21 (s, 2H), 4.36 (q, J = 7.1 Hz, 2H), 1.34 (t, J = 7.1 Hz, 3H). ^{13}C NMR (100 MHz, DMSO-d_6): δ 166.14, 158.91, 144.04, 141.62, 137.99, 133.42, 132.58, 131.28, 130.79, 130.64, 130.32, 129.54, 129.09, 118.51, 116.96, 112.23, 80.98, 60.94, 52.71, 16.36, 14.60.

Ethyl 2-(3-Cyanophenyl)-4-methyl-1-[(4-nitrobenzyl)oxy]-1*H*-imidazole-5-carboxylate (24v). Compound **24v** was prepared in the same manner as that described for **24c** to yield a white solid: 78.9%. Purity (HPLC): 98.1%. Mp 159.8−160.6 °C. ESI-HRMS calcd. for $C_{21}H_{18}N_4O_5$ $[M + H]^+$ 407.1350, found: 407.1398. ^{1}H NMR (600 MHz, DMSO-d_6): δ 8.09 (d, J = 8.6 Hz, 2H), 8.07−8.00 (m, 2H), 7.89 (dt, J = 7.7, 1.4 Hz, 1H), 7.61 (t, J = 7.8 Hz, 1H), 7.49 (d, J = 8.6 Hz, 2H), 5.29 (s, 2H), 4.35 (q, J = 7.1 Hz, 2H), 2.44 (s, 3H), 1.34 (t, J = 7.1 Hz, 3H). ^{13}C NMR (100 MHz, DMSO-d_6): δ 158.90, 148.31, 144.05, 141.55, 140.35, 133.51, 132.55, 131.48, 131.36, 130.37, 129.05, 123.80, 116.93, 112.25, 80.26, 60.97, 16.37, 14.59.

Ethyl 1-[(4-Cyanobenzyl)oxy]-2-(3-cyanophenyl)-4-methyl-1*H*-imidazole-5-carboxylate (24w). Compound **24w** was prepared in the same manner as that described for **24c** to yield a white solid: 81.6%. Purity (HPLC): 99.6%. Mp 174.4−176.3 °C. ESI-HRMS calcd. for $C_{22}H_{18}N_4O_3$ $[M + H]^+$ 387.1452, found: 387.1540. ^{1}H NMR (400 MHz, DMSO-d_6): δ 8.10−7.98 (m, 2H), 7.90 (dt, J = 7.8, 1.4 Hz, 1H), 7.72 (d, J = 8.2 Hz, 2H), 7.63 (t, J = 7.8 Hz, 1H), 7.41 (d, J = 8.2 Hz, 2H), 5.23 (s, 2H), 4.35 (q, J = 7.1 Hz, 2H), 2.44 (s, 3H), 1.33 (t, J = 7.1 Hz, 3H). ^{13}C NMR (100 MHz, DMSO-d_6): δ 158.89, 144.02, 141.55, 138.34, 133.52, 132.69, 132.53, 131.33, 131.11, 130.37, 129.06, 118.76, 118.54, 116.95, 112.49, 112.26, 80.69, 60.95, 16.37, 14.59.

Ethyl 1-[(2-Cyanobenzyl)oxy]-2-(3-cyanophenyl)-4-methyl-1*H*-imidazole-5-carboxylate (24x). Compound **24x** was prepared in the same manner as that described for **24c** to yield a white solid, yield: 73.9%. Purity (HPLC): 99.7%. Mp 186.8−188.4 °C. ESI-HRMS calcd. for $C_{22}H_{18}N_4O_3$ $[M + H]^+$ 387.1452, found: 387.1481. ^{1}H NMR (400 MHz, DMSO-d_6): δ 7.91−7.79 (m, 3H), 7.62−7.52 (m, 2H), 7.56−7.46 (m, 1H), 7.42 (td, J = 7.6, 1.3 Hz, 1H), 7.32 (d, J = 8.0 Hz, 1H), 5.32 (s, 2H), 4.35 (q, J = 7.1 Hz, 2H), 2.43 (s, 3H), 1.35 (t, J = 7.1 Hz, 3H). ^{13}C NMR (100 MHz, DMSO-d_6): δ 158.94, 144.29, 142.20,135.74, 133.45, 133.35, 133.21, 132.74, 132.50, 131.51, 130.77, 130.21, 128.94, 118.54, 116.98, 116.85, 113.50, 112.20, 79.22, 60.94, 16.38, 14.59.

Ethyl 1-[(3-Cyanobenzyl)oxy]-2-(3-cyanophenyl)-4-methyl-1*H*-imidazole-5-carboxylate (24y). Compound **24y** was prepared in the same manner as that described for **24c** to yield a white solid, yield: 76.8%. Purity (HPLC): 99.1%. Mp 172.3−173.7 °C. ESI-HRMS calcd. for $C_{22}H_{18}N_4O_3$ $[M + H]^+$ 387.1452, found: 387.1466. ^{1}H NMR (400 MHz, DMSO-d_6): δ 8.07−7.98 (m, 2H), 7.89 (dt, J = 7.7, 1.4 Hz, 1H), 7.75 (dt, J = 7.1, 1.7 Hz, 1H), 7.67−7.59 (m, 2H), 7.53−7.41 (m, 2H), 5.21 (s, 2H), 4.36 (q, J = 7.1 Hz, 2H), 2.44 (s, 3H), 1.35 (t, J = 7.1 Hz, 3H). ^{13}C NMR (100 MHz, DMSO-d_6): δ 158.92, 144.08, 141.72, 135.23, 134.59, 134.28, 133.53, 133.40, 132.61, 131.35, 130.34, 130.05, 129.05, 118.55, 116.93, 112.22, 111.81, 80.40, 60.95, 16.38, 14.59.

2-(3-Cyanophenyl)-1-methoxy-4-methyl-1*H*-imidazole-5-carboxylic acid (25a). A mixture of ethyl 2-(3-cyanophenyl)-1-methoxy-4-methyl-1*H*-imidazole-5-carboxylate **22a** (2.9 mmol), 1 M LiOH aqueous (11 mL), THF (5 mL), and ethanol (5 mL) was stirred at 50 °C for 6 h. The solvent was concentrated in a vacuum, and the residue was acidified with dilute hydrochloric acid to pH 1.

https://dx.doi.org/10.1021/acs.jmedchem.0c01524
J. Med. Chem. XXXX, XXX, XXX−XXX

The resulting precipitate was filtered, dried, and recrystallized with a mixture of methanol and ethyl acetate (2:1)[42] to yield the corresponding 2-(3-cyanophenyl)-1-methoxy-4-methyl-1*H*-imidazole-5-carboxylic acid **25a** as a white solid, yield: 91.2%. Purity (HPLC): 95.5%. Mp 203.7−205.3 °C. ESI-HRMS calcd. for $C_{13}H_{11}N_3O_3$ $[M - H]^-$ 256.0801, found: 256.0725. ^{1}H NMR (400 MHz, DMSO-d_6): δ 13.12 (s, 1H), 8.36−8.29 (m, 2H), 7.99−7.93 (m, 1H), 7.75 (t, J = 7.8 Hz, 1H), 3.97 (s, 3H), 2.40 (s, 3H). ^{13}C NMR (100 MHz, DMSO-d_6): δ 160.19, 143.51, 140.01, 133.65, 132.12, 130.86, 130.81, 129.23, 118.75, 117.59, 112.67, 67.59, 16.21.

1-(Allyloxy)-2-(3-cyanophenyl)-4-methyl-1*H*-imidazole-5-carboxylic acid (25d). Compound **25d** was prepared in the same manner as that described for **25a** to yield a white solid, yield: 91.5%. Purity (HPLC): 97.9%. Mp 176.6−178.2 °C. ESI-HRMS calcd. for $C_{15}H_{13}N_3O_3$ $[M - H]^-$ 282.0957, found: 282.0882. ^{1}H NMR (400 MHz, DMSO-d_6): δ 13.15 (s, 1H), 8.33 (t, J = 1.7 Hz, 1H), 8.30 (dt, J = 7.9, 1.4 Hz, 1H), 7.95 (dt, J = 7.8, 1.4 Hz, 1H), 7.74 (t, J = 7.9 Hz, 1H), 5.83 (ddt, J = 16.9, 10.3, 6.5 Hz, 1H), 5.40−5.26 (m, 2H), 4.67 (d, J = 6.5 Hz, 2H), 2.40 (s, 3H). ^{13}C NMR (100 MHz, DMSO-d_6): δ 160.30, 143.44, 140.76, 133.55, 132.35, 131.08, 130.88, 130.69, 129.55, 122.93, 118.72, 117.96, 112.52, 80.61, 16.25.

1-(Benzyloxy)-2-(3-cyanophenyl)-4-methyl-1*H*-imidazole-5-carboxylic acid (25k). Compound **25k** was prepared in the same manneras that described for **25a** to yield a white solid, yield: 90.2%. Purity (HPLC): 95.7%. Mp 195.3−197.4 °C. ESI-HRMS calcd. for $C_{19}H_{15}N_3O_3$ $[M - H]^-$ 332.1041, found: 332.1003. ^{1}H NMR (400 MHz, DMSO-d_6): δ 13.22 (s, 1H), 8.15−8.08 (m, 2H), 7.89 (dt, J = 7.7, 1.4 Hz, 1H), 7.69−7.60 (m, 1H), 7.37−7.30 (m, 1H), 7.31−7.24 (m, 2H), 7.24−7.18 (m, 2H), 5.13 (s, 2H), 2.43 (s, 3H). ^{13}C NMR (100 MHz, DMSO-d_6): δ 160.43, 143.65, 141.15, 133.27, 133.06, 132.45, 131.13, 130.61, 130.32, 129.82, 129.37, 128.84, 118.67, 117.65, 112.21, 81.72, 16.31.

2-(3-Cyanophenyl)-4-methyl-1-((4-methyl benzyl) oxy)-1*H*-imidazole-5-carboxylic acid (25s). Compound **25s** was prepared in the same manner as that described for **25a** to yield a white solid, yield: 81.2%. Purity (HPLC): 95.1%. Mp 168.2−169.8 °C. ESI-HRMS calcd. for $C_{20}H_{17}N_3O_3$ $[M - H]^-$ 346.1264, found: 346.1191. ^{1}H NMR (400 MHz, DMSO-d_6): δ 8.10−8.01 (m, 2H), 7.88 (dt, J = 7.7, 1.4 Hz, 1H), 7.63 (t, J = 7.9 Hz, 1H), 7.03 (d, 4H), 5.08 (s, 2H), 2.43 (s, 3H), 2.26 (s, 3H). ^{13}C NMR (100 MHz, DMSO-d_6): δ 167.82, 160.39, 143.68, 141.45, 139.51, 133.17, 132.56, 131.14, 130.67, 130.14, 130.00, 129.32, 118.69, 117.51, 112.04, 81.62, 21.25, 16.28.

1-[(4-Cyanobenzyl)oxy]-2-(3-cyanophenyl)-4-methyl-1*H*-imidazole-5-carboxylic acid (25w). Compound **25w** was prepared in the same manner as that described for **25a** to yield a white solid, yield: 92.4%. Purity (HPLC): 99.6%. Mp 201.5−202.3 °C. ESI-HRMS calcd. for $C_{20}H_{14}N_4O_3$ $[M - H]^-$ 357.1066, found: 357.0983. ^{1}H NMR (400 MHz, DMSO-d_6): δ 13.17 (s, 1H), 8.09−8.00 (m, 2H), 7.88 (dt, J = 7.7, 1.4 Hz, 1H), 7.71 (d, J = 8.1 Hz, 2H), 7.62 (t, J = 7.8 Hz, 1H), 7.40 (d, J = 8.2 Hz, 2H), 5.23 (s, 2H), 2.42 (s, 3H). ^{13}C NMR (100 MHz, DMSO-d_6): δ 160.35, 143.76, 141.22, 138.42, 133.34, 132.66, 132.44, 131.22, 131.10, 130.31, 129.23, 118.77, 118.57, 117.47, 112.46, 112.22, 80.56, 16.31.

ADP-Induced Rabbit PRP Aggregation Assay. All target compounds were evaluated for their antiplatelet potency in ADP-induced rabbit platelet-rich plasma (rPRP) aggregation.[11,22,23,44,56,75]

Preparation of Platelet-Rich Plasma (PRP). Blood was drawn from a rabbit carotid into a new tube containing 3.8% sodium citrate. The platelet-rich plasma (PRP) was obtained by centrifugation of the blood at 800 rpm for 10 min at room temperature, and the supernatant was carefully transferred to a fresh tube. Then, the remaining blood was again centrifuged at 3000 rpm for 10 min to prepare platelet-poor plasma (PPP), which was carefully transferred into a new tube.

Rabbit Platelet Aggregation 96-Well Assay. The rabbit platelet aggregation assay was performed in 96-well plates (COSTAR 3599) using a microplate reader.[75] In brief, PRP was added into a prewarmed 96-well microplate at 37 °C. Then, 15 μL of the test compounds at a 10× final concentration in NaCl was mixed with 135 μL of fresh PRP and incubated for 5 min. Following that incubation period, 15 μL of ADP (25 μM) was added to the reaction mix, leading to a final concentration of 2.27 μM ADP. The plates were then transferred to the microplate reader, and their absorbance was monitored every 1 min at 655 nm up to 6 min. The IC_{50} was further calculated on the basis of the aggregation of platelets (n = 3).

P2Y$_1$-Mediated Cytosolic Ca^{2+} Increase Assay on PRP. The ADP-dependent, P2Y$_1$-mediated increase in platelet cytosolic Ca^{2+} was measured by detecting changes in FLUO-4 fluorescence using a previously described method with minor modifications.[22,23,46,54,55] PRP was prepared as stated above, and it was added to HEPES−saline buffer (1:8 dilutions; 10 mM HEPES, 0.15 M NaCl, pH 7.4). Diluted PRP (70 μL, 8-fold) was incubated with 5 μM FLUO-4 AM (10 μL) in the presence of 0.02 U/mL apyrase (10 μL) and 10 μM indomethacin (10 μL) at 30 °C for 30 min. Then, 10 μL of the vehicle or the tested compounds at various concentrations was added into the mixture, which was incubated at 30 °C for 5 min. This mixture (110 μL) was added to 430 μL of HEPES−saline buffer, and the mixture was analyzed by a flow cytometer (BD FACSCalibur). After obtaining a 30 s baseline recording, the acquisition was paused, and then, 60 μL of ADP (5 μM final concentration) was quickly added, the mixture was mixed, and the acquisition resumed (total pause time less than 10 s). FLUO-4 fluorescence was monitored for 3 min. Fluo-4 fluorescence was plotted vs time, and the mean fluo-4 fluorescence of the baseline 30 s interval and of the 10 s poststimulant intervals were calculated. The cytosolic Ca^{2+} increase was calculated as the raise of the maximal poststimulant fluo-4 fluorescence over the baseline fluo-4 fluorescence. The percentage inhibition was calculated relative to ADP + vehicle (0% inhibition) and vehicle alone (100% inhibition): inhibition (%) = [(cytosolic Ca^{2+} increase $_{(ADP)}$ − cytosolic Ca^{2+} increase $_{(ADP+compound)}$)/(cytosolic Ca^{2+} increase $_{(ADP)}$ − cytosolic Ca^{2+} increase $_{(Black)}$)] × 100.

P2Y$_{12}$-Mediated Vasodilator-Stimulated Phosphoprotein (VASP) Phosphorylation Assay. This assay was measured by flow cytometry using a kit (BioCytex, Marseilles, France) according to the manufacturer's recommendations. First, 2 μL of the test compound solution or model (HEPES−saline) was added to each set of assay tubes, followed by 9 μL of PGE$_1$ or 9 μL of PGE$_1$/ADP.[23] Next, the citrated human whole blood was added to each tube and incubated for 10 min at room temperature.[23] Lastly, the samples were fixed, permeabilized, and labeled with a fluorescently conjugated monoclonal antibody (clone 16C2) directed against the serine 239 phosphorylated form of VASP, and CD61 was used as a platelet identifier.[23,56] The analysis was performed in a flow cytometer (BD FACSCalibur). The PGE$_1$-stimulated condition showed maximum VASP phosphorylation, and HEPES−saline buffer and ticagrelor were added as a control (no inhibition) and positive control, respectively. Furthermore, the agonist effects of the test compounds were checked using PGE$_1$ alone without ADP on samples.[22,23] The MFI was the mean fluorescence intensity of VASP phosphorylation,[49] and inhibition (%) = [(MFI$_{(PGE1)}$ − MFI$_{(PGE1+ADP+compound)}$)/(MFI$_{(PGE1)}$ − MFI$_{(Negative)}$)] × 100.

Xanthine Oxidase Inhibitory Activity. The XO inhibitory potency with xanthine as the substrate was assayed spectrophotometrically by measuring uric acid formation at 295 nm at 25 °C according to the procedure previously reported by us[52] with modifications. Febuxostat was used as a reference. XO (Sigma, X4875) was suspended in a buffer (0.1 M sodium pyrophosphate and 0.3 mM Na_2EDTA buffer, pH 8.3). The buffer (67 mL), enzyme solution (50/L, 40 μL), and sample (53 μL) or blank solution (the buffer) were added to 96-well plates (COSTAR 3599) and incubated at 25 °C for 15 min. Then, the mixture was added with substrate xanthine (40 μL, 500 μM) to the plates to a total volume of 200 μL, which was further scanned to measure the absorbance change immediately at 295 nm and at 30 s intervals for 2 min. All the tests were performed in triplicate. Compounds presenting inhibitory effects over 50% at a concentration of 10 μM were further tested at a wide range of concentrations to calculate their IC_{50} values using SPSS 20.0 software (SPSS Inc., Chicago, IL).

https://dx.doi.org/10.1021/acs.jmedchem.0c01524
J. Med. Chem. XXXX, XXX, XXX−XXX

Docking Studies. Molecular docking studies were performed using GLIDE (2016, Schrödinger Suite).[62] The crystal structures of $P2Y_1$ (PDB: 4XNW)[63] and $P2Y_{12}$ (PDB: 4NTJ)[64] were retrieved from the RCSB Protein Data Bank, which was further prepared using the Protein Preparation Wizard tool implemented in the Schrödinger suite by adding all hydrogen atoms as well as the missed side chains of residues and deleting all bound water. The ligands were built within Maestro BUILD (2016, Schrödinger Suite) and prepared by the LIGPREP module (2016, Schrödinger Suite).[62] The tautomeric forms of ligands, which include the keto and enol forms of ligands, were generated at a physiological pH (7.0 ± 2.0).[62] The Glide Grid was built using an inner box of dimensions 14 × 14 × 14 $Å^3$ around the centroid of the ligand, assuming that the ligands to be docked were of a size similar to that of the cocrystallized ligand. This docking methodology has been validated by extracting the crystallographic bound ligand and redocking it with the Glide module using extra precision (SP). Different docking poses of ligands were generated and analyzed for interpretation of the final results. Pymol[65] was used for graphic display.

Simulated Gastric and Intestinal Fluid Stability.[76,77] Incubations of tested compounds were performed at a concentration of 10 μM in simulated gastric and intestinal fluids. Then, these reaction solutions were kept at 37 °C and sampled hourly for 12 h. An aliquot (50 μL) of the mixtures was terminated hourly by the addition of 200 μL of ice-cold acetonitrile containing an internal standard (compound **24c**). After immediate mixing, extracts were centrifuged at 12 000 rpm for 10 min at 4 °C, and the supernatants were analyzed by HPLC.

Stability Studies in Plasma.[78,79] The plasma stability and metabolism of compounds **24w** and **25w** (initial concentration: 10 μM) were incubated in rabbit and rat plasma, respectively, and were placed in a water bath shaker at 37 °C. Reactions were terminated following 0, 5, 15, 30, and 45 min by ice-cold acetonitrile containing an internal standard (compound **24c**). After immediate mixing, the extracts were centrifuged at 12 000 rpm for 10 min at 4 °C, and the supernatants were analyzed by HPLC.

Stability Studies in Liver Microsomes.[80−83] The assay was performed using RLMs and HLMs, which were purchased from the Research Institute for Liver Diseases (Shanghai, China). The compounds (final concentration of 0.2 μM in 0.1% DMSO) were incubated with liver microsomes (0.50 mg/mL in 0.1 M PBS buffer (pH 7.4), 3.2 mM $MgCl_2$, and reduced nicotinamide adenine dinucleotide phosphate (NADPH, 1 mM)) at 37 °C. The reactions were stopped by transferring 50 μL of the reaction solutions into 200 μL of ice-cooled methanol containing 0.03 μM internal standard (compound **24c**) at 0, 10, 20, 30, 60, and 90 min. Then, the mixtures were vortex-mixed for 1 min and centrifuged at 12 000 rpm for 10 min, and supernatants were analyzed by LC−MS/MS.

CYP450 Inhibition Cocktail Assay.[68−70] The incubation mixture containing HLMs (final concentration: 0.5 mg/mL), $MgCl_2$ (final concentration: 3.2 mM), compounds **24w** or **25w** (final concentration: 10 μM), and specific CYP substrates in 0.1 M PBS buffer (pH 7.4) was preincubated for 5 min at 37 °C. Then, this reaction was initiated by the addition of NADPH solution (1 mM). The total content of organic solvent was maintained at <3%. The specific CYP substrates used in this cocktail assay included phenacetin, coumarin, tolbutamide, *S*-mephenytoin, dextromethorphan, chlorzoxazone, and testosterone (as probe substrates for enzymes of CYP1A2, CYP2A6, CYP2C9, CYP2C19, CYP2D6, CYP2E1, and CYP3A4, respectively). After a 120 min incubation at 37 °C, the reactions were quenched by the addition of cooled methanol with a mixture of internal standard (2-chloro-5-methoxyaniline hydrochloride, 0.5 μM). The mixture was vortex-mixed for 1 min and centrifuged at 12 000 rpm for 10 min, and the supernatants were used for a simultaneous analysis of the probe substrate metabolites (acetaminophen, 7-hydroxycoumarin, 4-hydroxytolbutamide, 4-hydroxymephenytoin, dextrorphan, 6-hydroxychlorzoxazone, and 6β-hydroxytestosterone) and internal standard by LC−MS/MS.

Rat Pharmacokinetic Studies.[84] Eighteen male Sprague-Dawley rats (300−320 g; Number of Approval from Ethics Committee: SYPU-IACUC-2019-9-23-201) were purchased from the Animal Center of Shenyang Pharmaceutical University (Shenyang, China). Animal maintenance and treatment met the protocols approved by the Ethics Review Committee for Animal Experimentation of Shenyang Pharmaceutical University. The rats had free access to food and water and were maintained on a 12 h light/dark cycle in a temperature- and humidity-controlled room for 1 week.[85,86]

A total of 18 Sprague-Dawley rats were randomly distributed into three experimental groups (n = 6 in each group). The oral groups were given compounds (**24w** or **25w**) suspended in 0.5% CMC-Na at an oral dose of 10 mg/kg, and the other group received a single intravenous injection of compound **25w** dissolved in a solution (saline/PBS/NaOH aqueous) at dose of 10 mg/kg. Whole blood samples (0.3 mL) were gathered into heparinized tubes *via* the suborbital vein after oral administration at 0.17, 0.33, 0.67, 1, 1.5, 2, 3, 4, 8, 16, and 24 h and after the intravenous administration at 0.083, 0.17, 0.33, 0.67, 1, 1.5, 2, 3, 4, 8, and 12 h. All blood samples were centrifuged (8000*g*, 10 min, 4 °C), and the resulting plasma samples were immediately stored at −80 °C until LC−MS analysis.

Acute Oral Toxicity Study. Healthy Kunming mice of both sexes (18−22 g; n = 8; Number of Approval from Ethics Committee: SYPU-IACUC-2019-5-29-202) were purchased from the Animal Center of Shenyang Pharmaceutical University (Shenyang, China). Animal maintenance and treatment met the protocols approved by the Ethics Review Committee for Animal Experimentation of Shenyang Pharmaceutical University. The mice had free access to food and water and were maintained on a 12 h light/dark cycle in a temperature- and humidity-controlled room for 1 week.[85−87]

After fasting for 12 h with free access to water prior to the experiment, four groups of animals (male control group, female control group, male test group, and female test group; n = 8) were used for acute oral toxicity study. The control groups were treated with the 0.5% CMC-Na, and the test groups were treated with a single dose (2000 mg/kg) of the test compound **24w**, which was suspended in a 0.5% CMC-Na solution. All treatments were intragastrically administered immediately after 12 h of fasting. The mice were observed continuously for any signs and symptoms of toxicity, and body weights of these mice were monitored every day over the 14 day period after treatment.[88]

Rat $FeCl_3$ Thrombosis Model. The $FeCl_3$-induced arterial thrombosis was instigated according to the previously described method with minor modifications.[11,72,73] Male Sprague-Dawley rats (300−320 g, n = 10; Number of Approval from Ethics Committee: SYPU-IACUC-2019-9-23-201) were purchased from the Animal Center of Shenyang Pharmaceutical University (Shenyang, China). Animal maintenance and treatment met the protocols approved by the Ethics Review Committee for Animal Experimentation of Shenyang Pharmaceutical University. The rats had free access to food and water and were maintained on a 12 h light/dark cycle in a temperature- and humidity-controlled room for 1 week.[85−87] Solutions of compound **24w**, ticagrelor, or model suspended in 0.5% CMC-Na were administered once a day for 7 consecutive days (including the last day) as a single oral dose of 10 mg/kg. Rats were anesthetized with urethane (1.25 g/kg, i.p.) and then placed on a heating pad to maintain body temperature. Through a median incision of the ventral side in the neck, a 1.5 cm long portion of the left carotid artery of rats was exposed *via* blunt dissection and carefully dissected clear of the vagus nerve and surrounding tissue. Then, this left carotid artery was put on a piece of plastic membrane (1.0 × 1.5 cm^2) to protect surrounding tissues.[11,72] A total of 1.5 h after drug administration, a strip of filter paper (0.8 × 1.0 cm^2) saturated with 20% $FeCl_3$ in water was placed on the anterior of the carotid artery to induce thrombosis formation.[11,72] Subsequently, the plastic membrane and filter paper were removed 2 h after drug administration and the right artery was cut immediately, gently blotted dry, and weighed.[11,72] The entire thrombosis was then scraped from artery, and the vessel wall was reweighed; the wet weight of thrombosis was obtained by subtraction.[11,72]

Rat Blood Loss Model. The rat blood loss model was performed as described previously with minor modifications.[11,44,48,72] Male

https://dx.doi.org/10.1021/acs.jmedchem.0c01524
J. Med. Chem. XXXX, XXX, XXX−XXX

Sprague-Dawley rats (300−320 g, n = 8; Number of Approval from Ethics Committee: SYPU-IACUC-2019-9-23-201) were purchased from the Animal Center of Shenyang Pharmaceutical University (Shenyang, China). Animal maintenance and treatment met the protocols approved by the Ethics Review Committee for Animal Experimentation of Shenyang Pharmaceutical University. The rats had free access to food and water and were maintained on a 12 h light/dark cycle in a temperature- and humidity-controlled room for 1 week. Compound **24w** and ticagrelor in 0.5% CMC-Na solution were administered by oral gavage at the 10 mg/kg dose. At 0.5 h after administration, the rats were anesthetized with urethane (1.25 kg, i.p.) and placed on a 37 °C heating pad to maintain body temperature with their tails straightened.[11,44,72] Then, 1.5 h after administration, rat tails were transected 4 mm from the tip with a scalpel blade and immediately immersed in a 20 mL graduated cylinder filled with 12 mL of saline held at 37 °C.[11,44,72] The observation period was stopped when no additional bloodstains were observed in a period of 30 seconds, and the bleeding time (including those of rebleeding) was recorded within 2 h.[11,44,72]

■ ASSOCIATED CONTENT

Supporting Information

The Supporting Information is available free of charge at https://pubs.acs.org/doi/10.1021/acs.jmedchem.0c01524.

Worksheet of molecular formula strings (XLSX)

Figures of HPLC spectra, ^{1}H and ^{13}C NMR spectra, HRMS spectra, and MS spectra (PDF)

■ AUTHOR INFORMATION

Corresponding Authors

Yanhua Mou − *Department of Pharmacology, Shenyang Pharmaceutical University, Shenhe District, Shenyang 110016, China*; Phone: 024-23986339; Email: mu_hua_jj@sina.com; Fax: 024-23986339

Shaojie Wang − *Key Laboratory of Structure-Based Drugs Design & Discovery of Ministry of Education, School of Pharmaceutical Engineering, Shenyang Pharmaceutical University, Shenhe District, Shenyang 110016, China*; Phone: (+86)24-23986421; Email: wangshaojie@syphu.edu.cn; Fax: (+86)24-23986421

Authors

Yu Lei − *Key Laboratory of Structure-Based Drugs Design & Discovery of Ministry of Education, School of Pharmaceutical Engineering, Shenyang Pharmaceutical University, Shenhe District, Shenyang 110016, China*

Bing Zhang − *Key Laboratory of Structure-Based Drugs Design & Discovery of Ministry of Education, School of Pharmaceutical Engineering, Shenyang Pharmaceutical University, Shenhe District, Shenyang 110016, China*; orcid.org/0000-0002-4427-8771

Dan Liu − *Shenyang Hinewy Pharmaceutical Technology Co., Ltd., Shenhe District, Shenyang 110016, China*

Jian Zhao − *Department of Pharmacology, Shenyang Pharmaceutical University, Shenhe District, Shenyang 110016, China*

Xiwen Dai − *Key Laboratory of Structure-Based Drugs Design & Discovery of Ministry of Education, School of Pharmaceutical Engineering, Shenyang Pharmaceutical University, Shenhe District, Shenyang 110016, China*

Jun Gao − *Key Laboratory of Structure-Based Drugs Design & Discovery of Ministry of Education, School of Pharmaceutical Engineering, Shenyang Pharmaceutical University, Shenhe District, Shenyang 110016, China*

Qing Mao − *Key Laboratory of Structure-Based Drugs Design & Discovery of Ministry of Education, School of Pharmaceutical Engineering, Shenyang Pharmaceutical University, Shenhe District, Shenyang 110016, China*

Yao Feng − *Key Laboratory of Structure-Based Drugs Design & Discovery of Ministry of Education, School of Pharmaceutical Engineering, Shenyang Pharmaceutical University, Shenhe District, Shenyang 110016, China*

Jiaxing Zhao − *Key Laboratory of Structure-Based Drugs Design & Discovery of Ministry of Education, School of Pharmaceutical Engineering, Shenyang Pharmaceutical University, Shenhe District, Shenyang 110016, China*

Fengwei Lin − *Key Laboratory of Structure-Based Drugs Design & Discovery of Ministry of Education, School of Pharmaceutical Engineering, Shenyang Pharmaceutical University, Shenhe District, Shenyang 110016, China*

Yulin Duan − *Key Laboratory of Structure-Based Drugs Design & Discovery of Ministry of Education, School of Pharmaceutical Engineering, Shenyang Pharmaceutical University, Shenhe District, Shenyang 110016, China*

Yan Zhang − *Department of Pharmacology, Shenyang Pharmaceutical University, Shenhe District, Shenyang 110016, China*

Ziyang Bao − *Key Laboratory of Structure-Based Drugs Design & Discovery of Ministry of Education, School of Pharmaceutical Engineering, Shenyang Pharmaceutical University, Shenhe District, Shenyang 110016, China*

Yuwei Yang − *Key Laboratory of Structure-Based Drugs Design & Discovery of Ministry of Education, School of Pharmaceutical Engineering, Shenyang Pharmaceutical University, Shenhe District, Shenyang 110016, China*

Complete contact information is available at: https://pubs.acs.org/10.1021/acs.jmedchem.0c01524

Author Contributions

‖Y.L. and B.Z. contributed equally to this work.

Notes

The authors declare no competing financial interest.

■ ACKNOWLEDGMENTS

The authors would like to thank Wei Zhang, Yanli Diao, and Jingyi Sun for their technical support in animal experiments.

■ ABBREVIATIONS USED

ACS, acute coronary syndromes; AMI, acute myocardial infarction; ADP, adenosine diphosphate; PCI, percutaneous coronary intervention; XO, xanthine oxidase; SAR, structure−activity relationships; rPRP, rabbit platelet-rich plasma; PK, pharmacokinetic; VASP, vasodilator-stimulated phosphoprotein; PGE_1, prostaglandin E_1; MFI, mean fluorescence intensity; PDB, protein data bank; PBS, phosphate buffer saline; NADPH, nicotinamide adenine dinucleotide phosphate; HLMs, human liver microsomes; RLMs, rat liver microsomes; Cl_{int}, intrinsic body clearance; C_{max}, peak plasma concentration; T_{max}, time to reach C_{max}; $t_{1/2}$, elimination half-life; $AUC_{0-\infty}$, area under the concentration−time curve; CLz, clearance; Vz, volume of distribution; F, absolute oral bioavailability; CYP450, cytochrome P450; $NaNO_2$, sodium nitrite; Me_3SiCl, chlorotrimethylsilane; NaI, sodium iodide; DMF, N,N-dimethylformamide; K_2CO_3, potassium carbonate; KI, potassium iodide; LiOH, lithuium hydroxide; Me_2SO_4, dimethyl sulfate

https://dx.doi.org/10.1021/acs.jmedchem.0c01524
J. Med. Chem. XXXX, XXX, XXX−XXX

REFERENCES

(1) Teng, R. Pharmacokinetic, pharmacodynamic and pharmacogenetic profile of the oral antiplatelet agent ticagrelor. *Clin. Pharmacokinet.* **2012**, *51*, 305−318.

(2) Schilling, U.; Dingemanse, J.; Ufer, M. Pharmacokinetics and pharmacodynamics of approved and investigational $P2Y_{12}$ receptor antagonists. *Clin. Pharmacokinet.* **2020**, *59*, 545−566.

(3) Naghavi, M.; et al. Global, regional, and national age-sex specific mortality for 264 causes of death, 1980−2016: a systematic analysis for the global burden of disease study 2016. *Lancet.* **2017**, *390*, 1151−1210.

(4) Hollopeter, G.; Jantzen, H. M.; Vincent, D.; Li, G.; England, L.; Ramakrishnan, V.; Yang, R. B.; Nurden, P.; Nurden, A.; Julius, D.; Conley, P. B. Identification of the platelet ADP receptor targeted by antithrombotic drugs. *Nature* **2001**, *409*, 202−207.

(5) Abbracchio, M. P.; Burnstock, G.; Boeynaems, J. M.; Barnard, E. A.; Boyer, J. L.; Kennedy, C.; Knight, G. E.; Fumagalli, M.; Gachet, C.; Jacobson, K. A.; Weisman, G. A. International Union of Pharmacology LVIII: update on the P2Y G protein-coupled nucleotide receptors: from molecular mechanisms and pathophysiology to therapy. *Pharmacol. Rev.* **2006**, *58*, 281−341.

(6) Dorsam, R. T.; Kunapuli, S. P. Central role of the $P2Y_{12}$ receptor in platelet activation. *J. Clin. Invest.* **2004**, *113*, 340−345.

(7) Gachet, C. Antiplatelet drugs: which targets for which treatments? *J. Thromb. Haemostasis* **2015**, *13*, S313−S322.

(8) Savi, P.; Herbert, J. M. Clopidogrel and ticlopidine: $P2Y_{12}$ adenosine diphosphate-receptor antagonists for the prevention of atherothrombosis. *Semin. Thromb. Hemostasis* **2005**, *31*, 174−183.

(9) Yuan, S.; Chan, H. C.; Vogel, H.; Filipek, S.; Stevens, R. C.; Palczewski, K. The molecular mechanism of $P2Y_1$ receptor activation. *Angew. Chem., Int. Ed.* **2016**, *55*, 10331−10335.

(10) Gao, N.; Hu, H. Z.; Zhu, M. X.; Fang, X.; Liu, S.; Gao, C.; Wood, J. D. The $P2Y_1$ purinergic receptor expressed by enteric neurones in guinea-pig intestine. *Neurogastroenterol. Motil.* **2006**, *18*, 316−323.

(11) Kong, D.; Xue, T.; Guo, B.; Cheng, J.; Liu, S.; Wei, J.; Lu, Z.; Liu, H.; Gong, G.; Lan, T.; Hu, W.; Yang, Y. Optimization of $P2Y_{12}$ antagonist ethyl 6-(4-((benzylsulfonyl) carbamoyl) piperidin-1-yl)-5-cyano-2-methylnicotinate (AZD1283) led to the discovery of an oral antiplatelet agent with improved druglike properties. *J. Med. Chem.* **2019**, *62*, 3088−3106.

(12) Cattaneo, M. New $P2Y_{12}$ inhibitors. *Circulation* **2010**, *121*, 171−179.

(13) Hagihara, K.; Kazui, M.; Ikenaga, H.; Nanba, T.; Fusegawa, K.; Takahashi, M.; Kurihara, A.; Okazaki, O.; Farid, N. A.; Ikeda, T. Comparison of formation of thiolactones and active metabolites of prasugrel and clopidogrel in rats and dogs. *Xenobiotica* **2009**, *39*, 218−226.

(14) Hulot, J. S.; Montalescot, G. Do we need a new $P2Y_{12}$ receptor antagonist? *Eur. Heart J.* **2020**, *41*, 3141−3143.

(15) Sugidachi, A.; Ohno, K.; Ogawa, T.; Jakubowski, J.; Hashimoto, M.; Tomizawa, A. A comparison of the pharmacological profiles of prasugrel and ticagrelor assessed by platelet aggregation, thrombus formation and haemostasis in rats. *Br. J. Pharmacol.* **2013**, *169*, 82−89.

(16) Baqi, Y.; Muller, C. E. Antithrombotic $P2Y_{12}$ receptor antagonists: recent developments in drug discovery. *Drug Discovery Today* **2019**, *24*, 325−333.

(17) Cristalli, G.; Podda, G. M.; Costanzi, S.; Lambertucci, C.; Lecchi, A.; Vittori, S.; Volpini, R.; Zighetti, M. L.; Cattaneo, M. Effects of 5′-phosphate derivatives of 2-hexynyl adenosine and 2-phenylethynyl adenosine on responses of human platelets mediated by P2Y receptors. *J. Med. Chem.* **2005**, *48*, 2763−2766.

(18) Qiao, J. X.; Wang, T. C.; Ruel, W. R.; Thibeault, C.; L'Heureux, A.; Schumacher, W. A.; Spronk, S. A.; Hiebert, S.; Bouthillier, G.; Lloyd, J.; Pi, Z.; Schnur, D. M.; Abell, L. M.; Hua, J.; Price, L. A.; Liu, E.; Wu, Q.; Steinbacher, T. E.; Bostwick, J. S.; Chang, M.; Zheng, J.; Gao, Q.; Ma, B.; McDonnell, P. A.; Huang, C. S.; Rehfuss, R.; Wexler, R. R.; Lam, P. Y. S. Conformationally constrained ortho-anilino diaryl ureas: discovery of 1-(2-(1′-neopentylspiro[indoline-3,4′-piperidine]-1-yl)phenyl)-3-(4-(trifluoromethoxy)phenyl)urea, a potent, selective, and bioavailable $P2Y_1$ antagonist. *J. Med. Chem.* **2013**, *56*, 9275−9295.

(19) Yang, W.; Wang, Y.; Lai, A.; Qiao, J. X.; Wang, T. C.; Hua, J.; Price, L. A.; Shen, H.; Chen, X.; Wong, P.; Crain, E.; Watson, C.; Huang, C. S.; Seiffert, D. A.; Rehfuss, R.; Wexler, R. R.; Lam, P. Y. S. Discovery of 4-aryl-7-hydroxyindoline based $P2Y_1$ antagonists as novel antiplatelet agents. *J. Med. Chem.* **2014**, *57*, 6150−6164.

(20) Bird, J. E.; Wang, X.; Smith, P. L.; Barbera, F.; Huang, C.; Schumacher, W. A. A platelet target for venous thrombosis? $P2Y_1$ deletion or antagonism protects mice from vena cava thrombosis. *J. Thromb. Thrombolysis* **2012**, *34*, 199−207.

(21) Chao, H.; Turdi, H.; Herpin, T. F.; Roberge, J. Y.; Liu, Y.; Schnur, D. M.; Poss, M. A.; Rehfuss, R.; Hua, J.; Wu, Q.; Price, L. A.; Abell, L. M.; Schumacher, W. A.; Bostwick, J. S.; Steinbacher, T. E.; Stewart, A. B.; Ogletree, M. L.; Huang, C. S.; Chang, M.; Cacace, A. M.; Arcuri, M. J.; Celani, D.; Wexler, R. R.; Lawrence, R. M. Discovery of 2-(phenoxypyridine)-3-phenylureas as small molecule $P2Y_1$ antagonists. *J. Med. Chem.* **2013**, *56*, 1704−1714.

(22) Yanachkov, I. B.; Chang, H.; Yanachkova, M. I.; Dix, E. J.; Berny-Lang, M. A.; Gremmel, T.; Michelson, A. D.; Wright, G. E.; Frelinger, A. L. New highly active antiplatelet agents with dual specificity for platelet $P2Y_1$ and $P2Y_{12}$ adenosine diphosphate receptors. *Eur. J. Med. Chem.* **2016**, *107*, 204−218.

(23) Chang, H.; Yanachkov, I. B.; Michelson, A. D.; Li, Y.; Barnard, M. R.; Wright, G. E.; Frelinger, A. L. Agonist and antagonist effects of diadenosine tetraphosphate, a platelet dense granule constituent, on platelet $P2Y_1$, $P2Y_{12}$ and $P2X_1$ receptors. *Thromb. Res.* **2010**, *125*, 159−165.

(24) Gremmel, T.; Yanachkov, I. B.; Yanachkova, M. I.; Wright, G. E.; Wider, J.; Undyala, V. V. R.; Michelson, A. D.; Frelinger, A. L.; Przyklenk, K. Synergistic inhibition of both $P2Y_1$ and $P2Y_{12}$ adenosine diphosphate receptors as novel approach to rapidly attenuate platelet-mediated thrombosis. *Arterioscler., Thromb., Vasc. Biol.* **2016**, *36*, 501−509.

(25) Zetterberg, F.; Svensson, P. State of affairs: Design and structure-activity relationships of reversible $P2Y_{12}$ receptor antagonists. *Bioorg. Med. Chem. Lett.* **2016**, *26*, 2739−2754.

(26) Doll, J. A.; Li, S.; Chiswell, K.; Roe, M. T.; Kosiborod, M.; Scirica, B. M.; Wang, T. Y. Clopidogrel reloading for patients with acute myocardial infarction already on clopidogrel therapy. *Eur. Heart J.* **2018**, *39*, 193−200.

(27) Huber, K.; Yasothan, U.; Hamad, B.; Kirkpatrick, P. Prasugrel. *Nat. Rev. Drug Discovery* **2009**, *8*, 449.

(28) McFadyen, J. D.; Schaff, M.; Peter, K. Current and future antiplatelet therapies: emphasis on preserving haemostasis. *Nat. Rev. Cardiol.* **2018**, *15*, 181−191.

(29) Columbo, J. A.; Lambour, A. J.; Sundling, R. A.; Chauhan, N. B.; Bessen, S. Y.; Linshaw, D. L.; Kang, R.; Riblet, N. B. V.; Goodney, P. P.; Stone, D. H. A meta-analysis of the impact of aspirin, clopidogrel, and dual antiplatelet therapy on bleeding complications in noncardiac surgery. *Ann. Surg.* **2018**, *267*, 1−10.

(30) Keating, G. M. Cangrelor: a review in percutaneous coronary intervention. *Drugs* **2015**, *75*, 1425−1434.

(31) Judge, H. M.; Buckland, R. J.; Jakubowski, J. A.; Storey, R. F. Cangrelor inhibits the binding of the active metabolites of clopidogrel and prasugrel to $P2Y_{12}$ receptors in vitro. *Platelets* **2016**, *27*, 191−195.

(32) Alexopoulos, D.; Pappas, C.; Sfantou, D.; Lekakis, J. Cangrelor in percutaneous coronary intervention: current status and perspectives. *J. Cardiovasc. Pharmacol. Ther.* **2018**, *23*, 13−22.

(33) Wallentin, L.; Becker, R. C.; Budaj, A.; Cannon, C. P.; Emanuelsson, H.; Held, C.; Horrow, J.; Husted, S.; James, S.; Katus, H.; Mahaffey, K. W.; Scirica, B. M.; Skene, A.; Steg, P. G.; Storey, R. F.; Harrington, R. A. Ticagrelor versus clopidogrel in patients with acute coronary syndromes. *N. Engl. J. Med.* **2009**, *361*, 1045−1057.

(34) Fan, Z. G.; Zhang, W. L.; Xu, B.; Ji, J.; Tian, N. L.; He, S. H. Comparisons between ticagrelor and clopidogrel following percutaneous coronary intervention in patients with acute coronary

https://dx.doi.org/10.1021/acs.jmedchem.0c01524
J. Med. Chem. XXXX, XXX, XXX−XXX

syndrome: a comprehensive meta-analysis. *Drug Des., Dev. Ther.* **2019**, *13*, 719−730.
(35) Franchi, F.; Rollini, F.; Rivas, A.; Wali, M.; Briceno, M.; Agarwal, M.; Shaikh, Z.; Nawaz, A.; Silva, G.; Been, L.; Smairat, R.; Kaufman, M.; Pineda, A.; Suryadevara, S.; Soffer, D.; Zenni, M. M.; Bass, T. A.; Angiolillo, D. J. Platelet inhibition with cangrelor and crushed ticagrelor in patients with ST-segment-elevation myocardial infarction undergoing primary percutaneous coronary intervention. *Circulation* **2019**, *139*, 1661−1670.
(36) Storey, R. F.; Gurbel, P. A.; Ten Berg, J.; Bernaud, C.; Dangas, G. D.; Frenoux, J. M.; Gorog, D. A.; Hmissi, A.; Kunadian, V.; James, S. K.; Tanguay, J. F.; Tran, H.; Trenk, D.; Ufer, M.; Van der Harst, P.; Van't Hof, A. W. J.; Angiolillo, D. J. Pharmacodynamics, pharmacokinetics, and safety of single-dose subcutaneous administration of selatogrel, a novel $P2Y_{12}$ receptor antagonist, in patients with chronic coronary syndromes. *Eur. Heart J.* **2020**, *41*, 3132−3140.
(37) Bach, P.; Boström, J.; Brickmann, K.; van Giezen, J. J. J.; Groneberg, R. D.; Harvey, D. M.; O'Sullivan, M.; Zetterberg, F. Synthesis, structure−property relationships and pharmacokinetic evaluation of ethyl 6-aminonicotinate sulfonylureas as antagonists of the $P2Y_{12}$ receptor. *Eur. J. Med. Chem.* **2013**, *65*, 360−375.
(38) Bach, P.; Antonsson, T.; Bylund, R.; Bjorkman, J. A.; Osterlund, K.; Giordanetto, F.; van Giezen, J. J.; Andersen, S. M.; Zachrisson, H.; Zetterberg, F. Lead optimization of ethyl 6-aminonicotinate acyl sulfonamides as antagonists of the $P2Y_{12}$ receptor. separation of the antithrombotic effect and bleeding for candidate drug AZD1283. *J. Med. Chem.* **2013**, *56*, 7015−7024.
(39) Rafeedheen, R.; Bliden, K. P.; Liu, F.; Tantry, U. S.; Gurbel, P. A. Novel antiplatelet agents in cardiovascular medicine. *Curr. Treat Options Cardiovasc Med.* **2015**, *17*, 1−15.
(40) Andre, P.; DeGuzman, F.; Haberstock-Debic, H.; Mills, S.; Pak, Y.; Inagaki, M.; Pandey, A.; Hollenbach, S.; Phillips, D. R.; Conley, P. B. Thienopyridines, but not elinogrel, result in off-target effects at the vessel wall that contribute to bleeding. *J. Pharmacol. Exp. Ther.* **2011**, *338*, 22−30.
(41) Bryant, J.; Post, J. M.; Alexander, S.; Wang, Y. X.; Kent, L.; Schirm, S.; Tseng, J. L.; Subramanyam, B.; Buckman, B.; Islam, I.; Yuan, S.; Sullivan, M. E.; Snider, M.; Morser, J. Novel $P2Y_{12}$ adenosine diphosphate receptor antagonists for inhibition of platelet aggregation (I): in vitro effects on platelets. *Thromb. Res.* **2008**, *122*, 523−532.
(42) Post, J. M.; Alexander, S.; Wang, Y. X.; Vincelette, J.; Vergona, R.; Kent, L.; Bryant, J.; Sullivan, M. E.; Dole, W. P.; Morser, J.; Subramanyam, B. Novel $P2Y_{12}$ adenosine diphosphate receptor antagonists for inhibition of platelet aggregation (II): pharmacodynamic and pharmacokinetic characterization. *Thromb. Res.* **2008**, *122*, 533−540.
(43) Boldron, C.; Besse, A.; Bordes, M. F.; Tissandie, S.; Yvon, X.; Gau, B.; Badorc, A.; Rousseaux, T.; Barre, G.; Meneyrol, J.; Zech, G.; Nazare, M.; Fossey, V.; Pflieger, A. M.; Bonnet-Lignon, S.; Millet, L.; Briot, C.; Dol, F.; Herault, J. P.; Savi, P.; Lassalle, G.; Delesque, N.; Herbert, J. M.; Bono, F. *N*-[6-(4-butanoyl-5-methyl-1*H*-pyrazol-1-yl)pyridazin-3-yl]-5-chloro-1-[2-(4-methyl piperazin-1-yl)-2-oxoethyl]-1*H*-indole-3-carboxamide (SAR216471), a novel intravenous and oral, reversible, and directly acting $P2Y_{12}$ antagonist. *J. Med. Chem.* **2014**, *57*, 7293−7316.
(44) Delesque-Touchard, N.; Pflieger, A. M.; Bonnet-Lignon, S.; Millet, L.; Salel, V.; Boldron, C.; Lassalle, G.; Herbert, J. M.; Savi, P.; Bono, F. SAR216471, an alternative to the use of currently available $P2Y_{12}$ receptor inhibitors? *Thromb. Res.* **2014**, *134*, 693−703.
(45) Baqi, Y.; Atzler, K.; Köse, M.; GläNzel, M.; Müller, C. E. High-affinity, non-nucleotide-derived competitive antagonists of platelet $P2Y_{12}$ receptors. *J. Med. Chem.* **2009**, *52*, 3784−3793.
(46) Hoffmann, K.; Baqi, Y.; Morena, M. S.; Glanzel, M.; Muller, C. E.; von Kugelgen, I. Interaction of new, very potent non-nucleotide antagonists with Arg256 of the human platelet $P2Y_{12}$ receptor. *J. Pharmacol. Exp. Ther.* **2009**, *331*, 648−655.
(47) Shan, J.; Zhang, B.; Zhu, Y.; Jiao, B.; Zheng, W.; Qi, X.; Gong, Y.; Yuan, F.; Lv, F.; Sun, H. Overcoming clopidogrel resistance: discovery of vicagrel as a highly potent and orally bioavailable antiplatelet agent. *J. Med. Chem.* **2012**, *55*, 3342−3352.
(48) Caroff, E.; Hubler, F.; Meyer, E.; Renneberg, D.; Gnerre, C.; Treiber, A.; Rey, M.; Hess, P.; Steiner, B.; Hilpert, K.; Riederer, M. A. 4-((R)-2-{[6-((S)-3-methoxypyrrolidin-1-yl)-2-phenylpyrimidine-4-carbonyl] amino}- 3-phosphonopropionyl) piperazine-1-carboxylic acid butyl ester (ACT-246475) and its prodrug (ACT-281959), a novel $P2Y_{12}$ receptor antagonist with a wider therapeutic window in the rat than clopidogrel. *J. Med. Chem.* **2015**, *58*, 9133−9153.
(49) Oliveira, S. D. S.; Oliveira, N. F.; Meyer-Fernandes, J. R.; Savio, L. E. B.; Ornelas, F. G. I.; Ferreira, Z. S.; Coutinho-Silva, R.; Silva, C. L. M. Increased expression of NTPDases 2 and 3 in mesenteric endothelial cells during schistosomiasis favors leukocyte adhesion through $P2Y_1$ receptors. *Vasc. Pharmacol.* **2016**, *82*, 66−72.
(50) Boyer, J. L.; Adams, M.; Ravi, R. G.; Jacobson, K. A.; Harden, T. K. 2-Chloro-N6-methyl-(N)-methanocarba-2′-deoxyadenosine-3′,5′-bisphosphate is a selective high affinity $P2Y_1$ receptor antagonist. *Br. J. Pharmacol.* **2002**, *135*, 2004−2010.
(51) Chen, S.; Zhang, T.; Wang, J.; Wang, F.; Niu, H.; Wu, C.; Wang, S. Synthesis and evaluation of 1-hydroxy/methoxy-4-methyl-2-phenyl-1*H*-imidazole-5-carboxylic acid derivatives as non-purine xanthine oxidase inhibitors. *Eur. J. Med. Chem.* **2015**, *103*, 343−353.
(52) Zhang, D.; Yang, T.; Lin, J. A novel xanthine oxidase inhibitor WSJ-557 study on pharmacokinetics and tissue distribution in rats by UPLC-MS/MS. *J. Chromatogr. B: Anal. Technol. Biomed. Life Sci.* **2019**, *1113*, 77−83.
(53) Wang, S. J. Compound with Xanthine Oxidase Inhibitory Activity and Salt Thereof, Preparation Method and Usage for the Same. Patent WO 2014023104A1, Feb 13, 2014.
(54) Aungraheeta, R.; Conibear, A.; Butler, M.; Kelly, E.; Nylander, S.; Mumford, A.; Mundell, S. J. Inverse agonism at the $P2Y_{12}$ receptor and ENT1 transporter blockade contribute to platelet inhibition by ticagrelor. *Blood* **2016**, *128*, 2717−2728.
(55) Cattaneo, M.; Lecchi, A.; Ohno, M.; Joshi, B. V.; Besada, P.; Tchilibon, S.; Lombardi, R.; Bischofberger, N.; Harden, T. K.; Jacobson, K. A. Antiaggregatory activity in human platelets of potent antagonists of the $P2Y_1$ receptor. *Biochem. Pharmacol.* **2004**, *68*, 1995−2002.
(56) Chang, H.; Yanachkov, I. B.; Dix, E. J.; Li, Y. F.; Barnard, M. R.; Wright, G. E.; Michelson, A. D.; Frelinger, A. L. Modified diadenosine tetraphosphates with dual specificity for $P2Y_1$ and $P2Y_{12}$ are potent antagonists of ADP-induced platelet activation. *J. Thromb. Haemostasis* **2012**, *10*, 2573−2580.
(57) Singh, D.; Silakari, O. Facile alkylation of 4-nitrobenzotriazole and its platelet aggregation inhibitory activity. *Bioorg. Med. Chem.* **2017**, *25*, 5260−5267.
(58) Bijak, M.; Szelenberger, R.; Dziedzic, A.; Saluk-Bijak, J. Inhibitory effect of flavonolignans on the $P2Y_{12}$ pathway in blood platelets. *Molecules.* **2018**, *23*, 374.
(59) Lortie, E.; Girard, F.; Boudreault, D.; Ruel, M.; Mansour, S.; Blais, N.; Hardy, J. F. Clopidogrel induces an acute hemostatic deficit and increases intra abdominal bleeding in rabbits. *Thromb. Res.* **2009**, *123*, 869−873.
(60) Söderlund, F.; Asztély, A.-K.; Jeppsson, A.; Nylander, S.; Berggren, A.; Nelander, K.; Castellheim, A.; Romlin, B. S. In vitro anti-platelet potency of ticagrelor in blood samples from infants and children. *Thromb. Res.* **2015**, *136*, 620−624.
(61) Bourguet, N.; Boulay-moine, D.; Miet, S.; Moulard, M. Evaluation of ELISA-based VASP assay with whole blood samples from several animal species, and compatibility with various platelet antagonists. *BIOCYTEX.* **2011**.
(62) *Glide*; Schrodinger, LLC: New York, NY, 2016.
(63) Zhang, D.; Gao, Z.-G.; Zhang, K.; Kiselev, E.; Crane, S.; Wang, J.; Paoletta, S.; Yi, C.; Ma, L.; Zhang, W.; Han, G. W.; Liu, H.; Cherezov, V.; Katritch, V.; Jiang, H.; Stevens, R. C.; Jacobson, K. A.; Zhao, Q.; Wu, B. Two disparate ligand-binding sites in the human $P2Y_1$ receptor. *Nature* **2015**, *520*, 317−321.
(64) Zhang, K.; Zhang, J.; Gao, Z. G.; Zhang, D.; Zhu, L.; Han, G. W.; Moss, S. M.; Paoletta, S.; Kiselev, E.; Lu, W.; Fenalti, G.; Zhang,

https://dx.doi.org/10.1021/acs.jmedchem.0c01524
J. Med. Chem. XXXX, XXX, XXX−XXX

W.; Muller, C. E.; Yang, H.; Jiang, H.; Cherezov, V.; Katritch, V.; Jacobson, K. A.; Stevens, R. C.; Wu, B.; Zhao, Q. Structure of the human $P2Y_{12}$ receptor in complex with an antithrombotic drug. *Nature* **2014**, *509*, 115−118.
(65) *The PyMOL Molecular Graphics System*, version 1.5.0.3; Schrödinger, LLC: New York.
(66) Paoletta, S.; Sabbadin, D.; von Kugelgen, I.; Hinz, S.; Katritch, V.; Hoffmann, K.; Abdelrahman, A.; Strassburger, J.; Baqi, Y.; Zhao, Q.; Stevens, R. C.; Moro, S.; Muller, C. E.; Jacobson, K. A. Modeling ligand recognition at the $P2Y_{12}$ receptor in light of X-ray structural information. *J. Comput.-Aided Mol. Des.* **2015**, *29*, 737−756.
(67) Knights, K. M.; Stresser, D. M.; Miners, J. O.; Crespi, C. L. *In vitro* drug metabolism using liver microsomes. *Curr. Protoc Pharmacol.* **2016**, *74*, 1−24.
(68) Kim, H. J.; Lee, H.; Ji, H. K.; Lee, T.; Liu, K. H. Screening of ten cytochrome P450 enzyme activities with 12 probe substrates in human liver microsomes using cocktail incubation and liquid chromatography−tandem mass spectrometry. *Biopharm. Drug Dispos.* **2019**, *40*, 101−111.
(69) Stresser, D. M.; Broudy, M. I.; Ho, T.; Cargill, C. E.; Blanchard, A. P.; Sharma, R.; Dandeneau, A. A.; Goodwin, J. J.; Turner, S. D.; Erve, J. C. L.; Patten, C. J.; Dehal, S. S.; Crespi, C. L. Highly selective inhibition of human cyp3aa in vitro by azamulin and evidence that inhibition is irreversible. *Drug Metab. Dispos.* **2004**, *32*, 105−112.
(70) Chen, N.; Yang, X. Y.; Guo, C. E.; Bi, X. N.; Chen, J. H.; Chen, H. Y.; Li, H. P.; Lin, H. Y.; Zhang, Y. J. The oral bioavailability, excretion and cytochrome P450 inhibition properties of epiberberine: an in vivo and in vitro evaluation. *Drug Des., Dev. Ther.* **2018**, *12*, 57−65.
(71) *The Hershberger Guideline, Performance-Based Test: OECD guideline for the testing of chemicals*. 2001; *601*, 858.
(72) Kim, C. W.; Yun, J. W.; Bae, I. H.; Park, Y. H.; Jeong, Y. S.; Park, J. W.; Chung, J. H.; Park, Y. H.; Lim, K. M. Evaluation of anti-platelet and anti-thrombotic effects of cilostazol with PFA-100(R) and Multiplate (R) whole blood aggregometer *in vitro*, *ex vivo* and $FeCl_3$-induced thrombosis models *in vivo*. *Thromb. Res.* **2011**, *127*, 565−570.
(73) Kim, S. K. Effects of modified Je-Ho-Tang on ferric chloride-induced thrombosis in a rat model and of peripheral circulatory disturbance in a mouse model. *Han'guk Eungyong Sangmyong Hwahakhoeji* **2010**, *53*, 842−846.
(74) Eckly, A.; Hechler, B.; Freund, M.; Zerr, M.; Cazenave, J. P.; Lanza, F.; Mangin, P. H.; Gachet, C. Mechanisms underlying $FeCl_3$-induced arterial thrombosis. *J. Thromb. Haemostasis* **2011**, *9*, 779−789.
(75) Chan, M. V.; Armstrong, P. C.; Warner, T. D. 96-well plate-based aggregometry. *Platelets* **2018**, *29*, 650−655.
(76) Megías, C.; Pedroche, J.; Yust, M. d. M.; Alaiz, M.; Girón-Calle, J.; Millán, F.; Vioque, J. Stability of sunflower protein hydrolysates in simulated gastric and intestinal fluids and Caco-2 cell extracts. *LWT - Food Science and Technology* **2009**, *42*, 1496−1500.
(77) Petersen, A. B.; Andersen, N. S.; Konotop, G.; Hanafiah, N. H.; Raab, M. S.; Kramer, A.; Clausen, M. H. Synthesis and formulation studies of griseofulvin analogues with improved solubility and metabolic stability. *Eur. J. Med. Chem.* **2017**, *130*, 240−247.
(78) Konsoula, R.; Jung, M. In vitro plasma stability, permeability and solubility of mercaptoacetamide histone deacetylase inhibitors. *Int. J. Pharm.* **2008**, *361*, 19−25.
(79) Xiang, Z.; Liu, J.; Sun, H.; Wen, X. Discovery of novel potent muscarinic M_3 receptor antagonists with proper plasma stability by structural recombination of marketed M_3 antagonists. *ChemMedChem* **2017**, *12*, 1173−1182.
(80) Lin, G.; Tang, J.; Liu, X. Q.; Jiang, Y.; Zheng, J. Deacetylclivorine: a gender-selective metabolite of clivorine formed in female Sprague-Dawley rat liver microsomes. *Drug Metab. Dispos.* **2007**, *35*, 607−613.
(81) Wang, K.; Wang, H.; Peng, Y.; Zheng, J. Identification of epoxide-derived metabolite(s) of benzbromarone. *Drug Metab. Dispos.* **2016**, *44*, 607−615.
(82) Chhonker, Y. S.; Sleightholm, R. L.; Murry, D. J. Bioanalytical method development and validation of moxidectin in plasma by LC-MS/MS: Application to in vitro metabolism. *Biomed. Chromatogr.* **2019**, *33*, e4389.
(83) Smith, R.; Jones, R. D.; Ballard, P. G.; Griffiths, H. H. Determination of microsome and hepatocyte scaling factors for *in vitro/in vivo* extrapolation in the rat and dog. *Xenobiotica* **2008**, *38*, 1386−1398.
(84) Bach, T.; Bae, S.; D'Cunha, R.; Winokur, P.; An, G. Development and validation of a simple, fast, and sensitive LC/MS/MS method for the quantification of oxfendazole in human plasma and its application to clinical pharmacokinetic study. *J. Pharm. Biomed. Anal.* **2019**, *171*, 111−117.
(85) Mao, Q.; Dai, X.; Xu, G.; Su, Y.; Zhang, B.; Liu, D.; Wang, S. Design, synthesis and biological evaluation of 2-(4-alkoxy-3-cyano) phenyl-6-oxo-1,6-dihydropyrimidine-5-carboxylic acid derivatives as novel xanthine oxidase inhibitors. *Eur. J. Med. Chem.* **2019**, *181*, 111558.
(86) Zhang, B.; Dai, X.; Bao, Z.; Mao, Q.; Duan, Y.; Yang, Y.; Wang, S. Targeting the subpocket in xanthine oxidase: Design, synthesis, and biological evaluation of 2-[4-alkoxy-3-(1*H*-tetrazol-1-yl) phenyl]-6-oxo-1,6-dihydropyrimidine-5-carboxylic acid derivatives. *Eur. J. Med. Chem.* **2019**, *181*, 111559.
(87) Gao, J.; Liu, X.; Zhang, B.; Mao, Q.; Zhang, Z.; Zou, Q.; Dai, X.; Wang, S. Design, synthesis and biological evaluation of 1-alkyl-5/6-(5-oxo-4,5-dihydro-1,2,4-oxadiazol-3-yl)-1*H*-indole-3-carbonitriles as novel xanthine oxidase inhibitors. *Eur. J. Med. Chem.* **2020**, *190*, 112077.
(88) Sun, L.; Dick, A.; Meuser, M. E.; Huang, T.; Zalloum, W. A.; Chen, C. H.; Cherukupalli, S.; Xu, S.; Ding, X.; Gao, P.; Kang, D.; De Clercq, E.; Pannecouque, C.; Cocklin, S.; Lee, K. H.; Liu, X.; Zhan, P. Design, synthesis, and mechanism study of benzenesulfonamide-containing phenylalanine derivatives as novel HIV-1 capsid inhibitors with improved antiviral activities. *J. Med. Chem.* **2020**, *63*, 4790−4810.

https://dx.doi.org/10.1021/acs.jmedchem.0c01524
J. Med. Chem. XXXX, XXX, XXX−XXX